

MECHANISTICAL STUDIES ON THE IRRADIATION OF METHANOL IN EXTRATERRESTRIAL ICES

CHRIS J. BENNETT,¹ SHIH-HUA CHEN,² BING-JIAN SUN,² AGNES H. H. CHANG,² AND RALF I. KAISER¹

Received 2006 August 30; accepted 2006 November 17

ABSTRACT

Pure ices of amorphous methanol, $\text{CH}_3\text{OH}(X^1A')$, were irradiated at 11 K by 5 keV electrons at 100 nA for 1 hr. These energetic electrons simulate electronic energy transfer processes that occur as interstellar ices, comets, and icy solar system bodies are subjected to irradiation from MeV ions and secondary electrons produced in this process. The results were analyzed quantitatively via absorption-reflection-absorption Fourier transform infrared (FTIR) spectroscopy, with the identification of new species aided by high-level electronic structure calculations. The unimolecular decomposition of methanol was found to proceed via the formation of (1) the hydroxymethyl radical, $\text{CH}_2\text{OH}(X^2A'')$, and atomic hydrogen, $\text{H}(^2S_{1/2})$, (2) the methoxy radical, $\text{CH}_3\text{O}(X^2A')$, plus atomic hydrogen, (3) formaldehyde, $\text{H}_2\text{CO}(X^1A_1)$ plus molecular hydrogen, $\text{H}_2(X^1\Sigma_g^+)$, and (4) the formation of methane, $\text{CH}_4(X^1A_1)$, together with atomic oxygen, $\text{O}(^1D)$. The accessibility of the last channel indicates that the reverse process, oxygen addition into methane to form methanol, should also be feasible. A kinetic model is presented for the decomposition of methanol into these species, as well as the formyl radical, $\text{HCO}(X^2A')$, and carbon monoxide, $\text{CO}(X^1\Sigma^+)$. During the subsequent warming up of the sample, radicals previously generated within the matrix were mobilized and found to recombine to form methyl formate, $\text{CH}_3\text{OCHO}(X^1A')$, glycolaldehyde, $\text{CH}_2\text{OHCHO}(X^1A')$, and ethylene glycol, $\text{HOCH}_2\text{CH}_2\text{OH}(X^1A)$. Upper limits for the production of these species by the recombination of neighboring radicals produced during irradiation as well as during the warm-up procedure are presented. The generation of these molecules by irradiation of ices in the solid state and their subsequent sublimation into the gas phase can help explain their high abundances as observed toward hot molecular cores and underlines their importance in astrobiology.

Subject headings: cosmic rays — ISM: molecules — methods: laboratory — molecular processes — planets and satellites: general

1. INTRODUCTION

One of the recent challenges in astrochemistry is to explain the production pathways for the increasingly complex molecules continuing to be discovered in the interstellar medium. Complex organic molecules of particular astrobiological interest include two groups of structural isomers (molecules with the same chemical formula, but different chemical structures). These are three isomers from both the $\text{C}_2\text{H}_4\text{O}$ group (acetaldehyde [CH_3CHO], vinyl alcohol [$\text{H}_2\text{C}=\text{CHOH}$], and ethylene oxide [$\text{C}_2\text{H}_4\text{O}$]) and the $\text{C}_2\text{H}_4\text{O}_2$ group (glycolaldehyde [CH_2OHCHO], methyl formate [CH_3OCHO], and acetic acid [CH_3COOH]); all these molecules have now been identified in hot molecular cores (Gottlieb 1973; Brown et al. 1975; Dickens & Irvine 1997; Mehringer et al. 1997; Hollis et al. 2000; Turner & Apponi 2001).

Interestingly, chemical models of hot molecular cores rely on rapid, high-temperature gas-phase chemistry to explain the abundance of these molecules; the physical processes are thought to be triggered by the sublimation of methanol-rich icy grains. This process is thought to provide high abundances of large organic molecules for periods up to 10^4 – 10^5 yr (Charnley et al. 1992; Rodgers & Charnley 2001). It has recently been noted, however, that molecules subliming from these grains will have lifetimes of only a few hundred years before collapsing into the protostar; unlikely enough time to form complex molecules by methanol-induced gas-phase chemistry (Schöier et al. 2002; Rodgers & Charnley 2003). In addition, the majority of the reaction pathways to form these molecules via gas-phase processes involve ion-molecule reactions, processes that have not all been studied experimen-

tally. Recent studies indicated that ion-molecule reactions of, for instance, CH_3OH_2^+ , already included in these models, proceed slower than predicted and cannot explain the observed abundances of the $\text{C}_2\text{H}_4\text{O}$ and $\text{C}_2\text{H}_4\text{O}_2$ isomers quantitatively (Horn et al. 2004). Thus, one of our main research goals is to establish alternative pathways to form these complex molecules, which are proposed to be formed within the icy grains themselves in cold molecular clouds and are detected as the ices sublime when the protostar develops. It is well known that the icy grains present within interstellar clouds are subjected to irradiation from Galactic cosmic rays (GCRs) throughout the lifetime of an interstellar cloud of about $(4\text{--}6) \times 10^8$ yr (Jones 2005). These GCR particles can have high kinetic energies up to the GeV energy range; for instance, values assumed in the literature for the flux of 1 MeV protons include: $\phi = 10$ protons $\text{cm}^{-2} \text{s}^{-1}$ (Strazzulla & Johnson 1991), $\phi = 0.6\text{--}3$ protons $\text{cm}^{-2} \text{s}^{-1}$ (Jenniskens et al. 1993), and $\phi = 1.0$ protons $\text{cm}^{-2} \text{s}^{-1}$ (Mennella et al. 2003). Chemically speaking, the cosmic-ray radiation field comprises about 98% protons (p , H^+) and 2% helium nuclei (α -particles, He^{2+}). These GCR particles can also induce an internal ultraviolet field, holding a fluence $\phi = 10^3$ photons $\text{cm}^{-2} \text{s}^{-1}$, even deep within cold molecular clouds (Prasad & Tarfdar 1983).

Methanol itself has long been known to be a constituent of the icy mantle on interstellar grains; however, its abundance relative to water is highly variable on which band is used to derive the column density (Grim et al. 1991; Palumbo et al. 1999). A recent survey of 23 infrared sources carried out by Gibb et al. (2004) using the *Infrared Space Observatory* (ISO) found large discrepancies for the derived methanol abundance reported, in particular, between when the $3.53 \mu\text{m}$ (2828 cm^{-1} [ν_3 , C-H stretch]) and $3.95 \mu\text{m}$ (2531 cm^{-1} [$\nu_6+\nu_{11}$, combination band]) bands were used. In the case of the high-mass young stellar object (YSO) Orion BN, an upper limit of 4% (relative to water) is derived using

¹ Department of Chemistry, University of Hawai'i at Manoa, Honolulu, HI; kaiser@gold.chem.hawaii.edu.

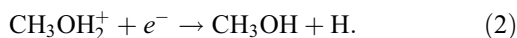
² Department of Chemistry, National Dong Hwa University, Shou-Feng, Hualien, Taiwan.

the 3.53 μm band, whereas the 3.95 μm band gives an upper limit of 27%. On the other hand, for the intermediate-mass YSO AFGL 989 using the 3.53 μm band gives an abundance of about 23%, whereas in this case, the 3.95 μm band gives a value of only 1.7%. Despite these inconsistencies, a general trend between methanol abundance and the amount of energetic processing occurring within the astronomical environment was suggested. The ices in the line of sight from Elias 3-16 are thought to be in a quiescent environment from which a methanol abundance of only 3% was reported. On the other hand, the ices surrounding high-mass YSOs, which are thought to highly process their surrounding ices such as W33A and AFGL 7009S, have abundances as high as 15%–30% relative to water.

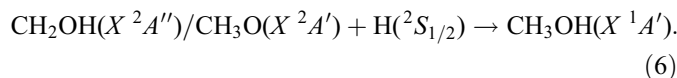
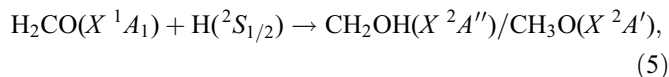
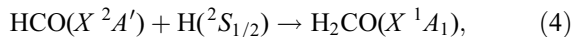
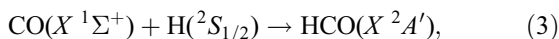
The formation of methanol itself is still a matter of dispute; the main gas-phase formation process is considered to be through radiative association of a methyl ion with water



Followed by dissociative recombination of the CH_3OH_2^+ ion,



Chemical models of dense molecular cores fall short on reproducing the methanol abundances, even without incorporating the recently determined rate constant for reaction (1), which was found to be 3 orders slower than predicted at 10 K (Maret et al. 2005). Alternative production routes for methanol that have been suggested include its formation on the surface of interstellar grains by the successive hydrogenation of carbon monoxide:



However, this process is not very efficient at forming methanol at low temperatures, as revealed by recent experiments by Hiraoka et al. (2005). At low temperatures, the thermalized hydrogen atoms would not bear enough kinetic energy to efficiently overcome the entrance barriers that may be present; reaction (3) has a computed barrier of 11.2 kJ mol^{-1} (0.12 eV), reported by Bennett et al. (2005), and reaction (5) of 21.2 kJ mol^{-1} (via $\text{CH}_3\text{O}[X^2A']$) or 48.2 kJ mol^{-1} (through $\text{CH}_2\text{OH}[X^2A'']$) (Chang & Lin 2004). Alternatively, methanol could actually be synthesized within these interstellar ices as they are subjected to MeV ions as well as UV photons. Laboratory experiments on the irradiation of binary ice mixtures containing water and carbon monoxide (5 : 1), as well as water and methane (10 : 1) both report the production of methanol (Hudson & Moore 1999; Wada et al. 2006). The fact that higher methanol abundances are reported toward the center of YSOs is consistent with methanol subliming from grains, and the higher reported abundances in more processing environments may indicate irradiation-driven solid-state formation (Gibb et al. 2004; Maret et al. 2005).

Methanol is also a known component of comets and other solar system bodies. Mumma et al. (2005) compared the compositions of volatiles from Oort cloud comets, finding methanol abundance to be typically of 1%–3% relative to water. Methanol

has also been detected on a number of other solar system bodies, such as the centaur 5145 Pholus (Cruikshank et al. 1998) and has been incorporated into models of reflectance spectra for outer solar system bodies (Cruikshank et al. 2003).

Although the effects of radiolysis by both ions and UV photons has been studied on pure and mixed methanol systems, the identification of several previously assigned species still needs to be substantiated, and their mechanistic formation pathways elucidated. Allamandola et al. (1988) exposed a thin layer ($<1 \mu\text{m}$) ice of water and methanol (2:1) to UV photons generated by a hydrogen discharge lamp ($\Phi \sim 2 \times 10^{15}$ photons s^{-1} , predominantly $\text{Ly}\alpha$ [10.2 eV]) for 45 minutes. The following products were identified by mid-infrared spectroscopy: formaldehyde (at 1720 and 1500 cm^{-1}), methane (3012 and 1304 cm^{-1}), carbon monoxide (2137 cm^{-1}), carbon dioxide (2343 and 657 cm^{-1}), and the formyl radical (1850 cm^{-1}).

Gerakines et al. (1996) exposed a pure methanol ice sample of about 0.1 μm thickness to 1 hr of UV irradiation from a microwave discharge flow lamp (typically the flux of photons is estimated to be 10^{15} photons $\text{cm}^{-2} \text{s}^{-1}$ with energies greater than 6 eV, but predominantly the photons produced are $\text{Ly}\alpha$ photons). The products were studied via mid-infrared spectroscopy, whereby they were also able to identify formaldehyde (at 1720, 1494, and 1244 cm^{-1}), methane (1302 and 3011 cm^{-1}), carbon monoxide (2138 cm^{-1} , and its ^{13}C isotopomer at 2092 cm^{-1}), carbon dioxide (2342 and 655 cm^{-1} , ^{13}C at 2278 cm^{-1}), and the formyl radical (1850 and 1863 cm^{-1}). In addition, they also reported absorptions from the hydroxymethyl radical (1197 and 1352 cm^{-1}) and methyl formate (1718, 1160, and 910 cm^{-1}) and assigned a band appearing at 1088 cm^{-1} to “alcohols.”

Baratta et al. (1994) used 3 keV He^+ ions to bombard pure methanol as well as binary 1:1 water and methanol samples a few hundred angstroms thick, exposing them to a dose up to 60 eV per 16 amu (atomic mass units). In accordance with studies by UV photolysis, they were also able to identify formaldehyde (1720 cm^{-1}), methane (1308 cm^{-1}), carbon monoxide (2136 cm^{-1}), and carbon dioxide (2344 cm^{-1}). Although they were unable to identify the formyl radical, additional assignments were made to the production of water (1655 cm^{-1} and inferred by modification to the OH-stretching band of methanol) as well as to acetone (1720, 1444, 1232, and 1090 cm^{-1}).

Moore et al. (1996) exposed ice films of about 4 μm thickness to a dose of 34 eV molecule $^{-1}$ by irradiation from a 1 MeV proton beam. Again, absorptions were reported of the formation of formaldehyde (1721, 1497, and 1246 cm^{-1}), methane (1302 cm^{-1}), carbon monoxide (2134 cm^{-1}), carbon dioxide (2339 and 650 cm^{-1}), and the formyl radical (1844 cm^{-1}). They found no evidence for water and reassigned the band occurring at 1090 cm^{-1} to ethanol, rather than acetone. However, they did attribute a broad feature between 532–516 cm^{-1} to acetone, whose presence was also inferred by data from their mass spectrometer incorporated into the apparatus that detected fragmentation patterns at m/e 58 and 43, consistent with the presence of this molecule. They also noted that after heating the sample, features that resembled those of ethylene glycol could be identified.

Palumbo et al. (1999) irradiated pure methanol with 3 keV He^+ ions at a dose of 52 eV per 16 amu but did not report new features: formaldehyde (1720 cm^{-1}), methane (1305 and 3010 cm^{-1}), carbon monoxide (2136 cm^{-1}), carbon dioxide (2344 and 660 cm^{-1}), as well as water (1655 cm^{-1}), and they noted that acetone likely contributed to the 1720 cm^{-1} feature.

Hudson & Moore (2000) carried out experiments on pure methanol ices using 0.8 MeV protons, with several changes to their interpretation of the previously assigned bands. They report some of

the previously detected species, such as formaldehyde (1712, 1499, and 1248 cm^{-1}), methane (1303 cm^{-1}), carbon monoxide (2135 cm^{-1}), carbon dioxide (2341 and 654 cm^{-1}), and the formyl radical (1848 cm^{-1}). However, they found no evidence for ethanol, water, or acetone within their experiments. Instead, they assigned absorptions appearing at 1088, 1046, 885, 861, and 524 cm^{-1} to ethylene glycol and bands appearing at 1589, 1384, and 1353 cm^{-1} to the formate ion.

Baratta et al. (2002) compared the effects of UV photons ($\text{Ly}\alpha$) and 30 keV He^+ ion irradiation on methanol samples around 74 nm thick. They reported a quantitative comparison of the irradiation sources on the destruction of methanol, as well as the production of formaldehyde, methane, carbon monoxide, and carbon dioxide. Recent studies on the irradiation effects of 30 keV He^+ ions on methanol ices by Brunetto et al. (2005), which focused on a different spectral region (the near-infrared), questioned the formation of ethylene glycol, whose absorption features in this region could not be identified.

Thus, it is clear that further work is needed to establish not only what molecules are present in these ices, but also what their production mechanisms are and to what extent they can be justified. To our knowledge, however, no previous experiments studying the irradiation effects of high-energy electrons on solid methanol under ultrahigh vacuum conditions have been carried out. The choice of energetic electrons as an irradiation source serves to simulate not only the irradiation of icy surfaces by energetic electrons (e.g., the Jovian system), but also the effects of δ -electrons released in the track of MeV ions (see Bennett et al. [2005] for a detailed discussion). The linear energy transfer through electronic interactions to the ice sample from keV electrons is also of the same order to that of MeV H^+ and He^+ ions (e.g., Johnson 1990).

2. EXPERIMENTAL

Briefly, an ultrahigh vacuum (UHV) chamber is evacuated down to a base pressure of typically 5×10^{-11} torr using oil-free magnetically suspended turbomolecular pumps. A closed cycle helium refrigerator is used to cool a highly polished silver (111) mono crystal to 11.4 ± 0.3 K, which is held in the center of the chamber and is freely rotatable. The methanol (CH_3OH) frost was prepared by depositing methanol (99.9% Fisher Chemicals, further purified by a foreline liquid nitrogen cold trap) for 1 minute at a background pressure of 10^{-8} torr onto the cooled silver crystal. A Nicolet 510 DX Fourier transform infrared spectrometer (242 scans over 5 minutes from 5000–400 cm^{-1} , resolution 2 cm^{-1}) running in absorption-reflection-absorption mode (reflection angle $\alpha = 75^\circ$) is used to monitor the condensed sample. A quadrupole mass spectrometer (Balzer QMG 420) operating in residual gas analyzer mode with the electron impact ionization energy at 90 eV allows us to detect any species in the gas phase during the experiment.

The methanol samples were irradiated isothermally at 11 K with 5 keV electrons generated with an electron gun (Specs EQ 22/35) at beam currents of 100 nA for 1 hr by scanning the electron beam over an area of 3.0 ± 0.4 cm^2 . In theory this would mean during the irradiation the sample would be exposed to a total of 2.2×10^{15} electrons (7.5×10^{14} electrons cm^{-2}); however, not all of the electrons generated by our electron gun actually reach the target; the manufacturer states an extraction efficiency of 78.8%, meaning the actual number of electrons that hit the sample is reduced to 1.8×10^{15} electrons (5.9×10^{14} electrons cm^{-2}). After the irradiation is complete, the sample is then left isothermally for 1 hr, before being heated to 300 K at a rate of 0.5 K minute^{-1} .

Figure 1 (*dashed line*) depicts a typical infrared spectrum of the condensed methanol frost prior to the irradiation at 11 K; the

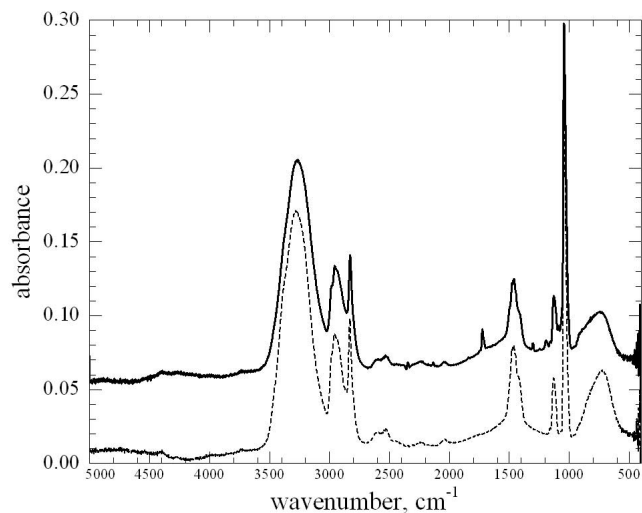


FIG. 1.—Comparison of the infrared spectra of the methanol frost at 11 K before irradiation (*dashed line*) and after irradiation (*solid line*; offset by 0.05). The corresponding assignments for methanol before irradiation are given in Table 1 and are given for the products identified after irradiation in Table 2.

assignments of these bands are presented in Table 1. Previous studies showed that when methanol is condensed below 128 K, it should form an amorphous solid, which is stable until around 145 K, transforming into the α -phase (Lucas et al. 2005). The column density of methanol (molecules cm^{-2}) can be calculated via a modified Lambert-Beers relationship as in equation (7).

$$N = \frac{\ln 10}{2} \cos \alpha \frac{\int_{\tilde{\nu}_1}^{\tilde{\nu}_2} A(\tilde{\nu}) d\tilde{\nu}}{A}, \quad (7)$$

where the division by a factor of 2 corrects for the ingoing and outgoing infrared beam, α is the angle between the normal of the surface mirror and the infrared beam, $\int_{\tilde{\nu}_1}^{\tilde{\nu}_2} A(\tilde{\nu}) d\tilde{\nu}$ is the integral of the infrared absorption feature for our sample (cm^{-1}), and A is the integral absorption coefficient (cm molecule^{-1}), often referred to as an “ A value.” Using a recently determined A value from Palumbo et al. (1999) of 1.3×10^{-17} cm molecule^{-1} for the band appearing at 1037 cm^{-1} (ν_8 and ν_{11} fundamentals), we derive a column density of $(1.64 \pm 0.04) \times 10^{17}$ molecules cm^{-2} . Taking a density of 1.020 g cm^{-3} (Tauer & Lipscomb 1952), we can derive a thickness of 85 ± 2 nm. The electron trajectories were simulated using the CASINO code (Drouin et al. 2001). The results indicate that the distribution maximum for the energy of electrons after they have been transmitted through the sample is 4.61 ± 0.01 keV. This means that they transfer a total of 390 ± 10 eV per electron into the sample. This value corresponds to an average linear energy transfer (LET) of 4.6 ± 0.2 keV μm^{-1} and, therefore, exposes our sample to an *average* dose of 1.4 ± 0.2 eV per molecule.

3. THEORETICAL CALCULATIONS

The molecules for which the electronic structures have been investigated can be placed into two groups: those that we expect to be produced from the radiolysis of methanol itself (Fig. 2; Table A6) and those that we expect to form from the recombination of radicals generated in situ, in addition to the structures of molecules reported in previous studies (Fig. 3; Table A7). The molecules were studied computationally by employing the hybrid density functional B3LYP (Lee et al. 1988; Becke 1993) with the 6-311G(d,p) basis functions to obtain the optimized molecular

TABLE 1
BAND POSITIONS OF THE UNDERLYING GAUSSIANS USED TO FIT THE OBSERVED INFRARED ABSORPTIONS OF THE METHANOL FROST AND ASSIGNMENTS,
ALONG WITH CHARACTERIZATIONS AND BAND ASSIGNMENTS COMPARED TO SEVERAL PREVIOUS STUDIES

ASSIGNMENT	CHARACTERIZATION	BAND POSITION (cm ⁻¹)					
		This Work	Amorphous 93 K ^a	Crystalline 93 K ^a	Crystalline 15 K ^b	Ar Matrix 15 K ^c	Liquid ^d
$\nu_2/\nu_9 + \nu_4/\nu_6/\nu_{10}$	Combination	4402			4420		
$\nu_2/\nu_9 + \nu_7?$	Combination	4270			4097?		
$\nu_2/\nu_9 + \nu_8$	Combination	3991			4000		
?	?	3856					
?	?	3735					
ν_1	Fundamental	3426, 3389, 3274, 3187, 3080	3235	3443, 3284, 3187	3284, 3194	3672, 3667	3483, 3363, 3349, 3145, 3038
ν_2	Fundamental	2987	2982	2982		3006	2983
ν_9	Fundamental	2961	2951	2955	2968	2962	2946
$2\nu_4?$	Overtone?					2956	
$\nu_4 + \nu_5/\nu_4 + \nu_{10}/\nu_5 + \nu_{10}/2\nu_4/2\nu_{10}/2\nu_5$	Combination/Overtone	2920		2912	2903	2930, 2921, 2915, 2908	2917
$2\nu_5/2\nu_{10}$	Overtone	2864				(2893) ^e	2872
ν_3	Fundamental	2828	2828	2829	2831	2848	2833
$2\nu_6$	Overtone	2811					2809
$\nu_4 + \nu_{11}/\nu_7 + \nu_4/\nu_6/\nu_{10}$	Combination	2601			2581		2601
$\nu_6 + \nu_{11}$	Combination	2527					2520
$\nu_6 + \nu_8$	Combination	2443					2440
$2\nu_{11}/2\nu_7$	Overtone	2237				2226	2226
$2\nu_8$	Overtone	2040			2057	2054	2046
?	?	1771					
$\nu_8 + \nu_{12}?$	Combination	1495		1514	1508		1555
ν_4	Fundamental	1478		1470		1473	1470
ν_{10}	Fundamental	1461	1450, 1451	1458	1451	1466	
ν_5	Fundamental	1444		1445		1452	1451
ν_6	Fundamental	1428	1415	1426	1411		1415
$\nu_{11} + \nu_{12}?$	Combination?	1407				(1414) ^e	
$2\nu_{12}$	Overtone	1188	1256	1256	1250		1208?
ν_7	Fundamental	1157, 1137, 1128, 1120, 1113	1124	1162, 1146, 1142	1129	1145	1117
ν_{11}	Fundamental	1047		1046		1077	1088
ν_8	Fundamental	1041, 1031	1032	1029	1032	1034, 1028	1039, 1031
ν_8	Fundamental (¹³ C)	1011				1019	1019
ν_{12}	Fundamental	834, 713	730	790, 685	782, 694	272	677, 633, 614, 400

^a Values from Falk & Whalley (1961).

^b Values from Wen et al. (1998) via electron-energy-loss spectroscopy (EELS).

^c Values from Serrallach et al. (1974).

^d Values from Bertie & Zhang (1997).

^e Gas-phase value.

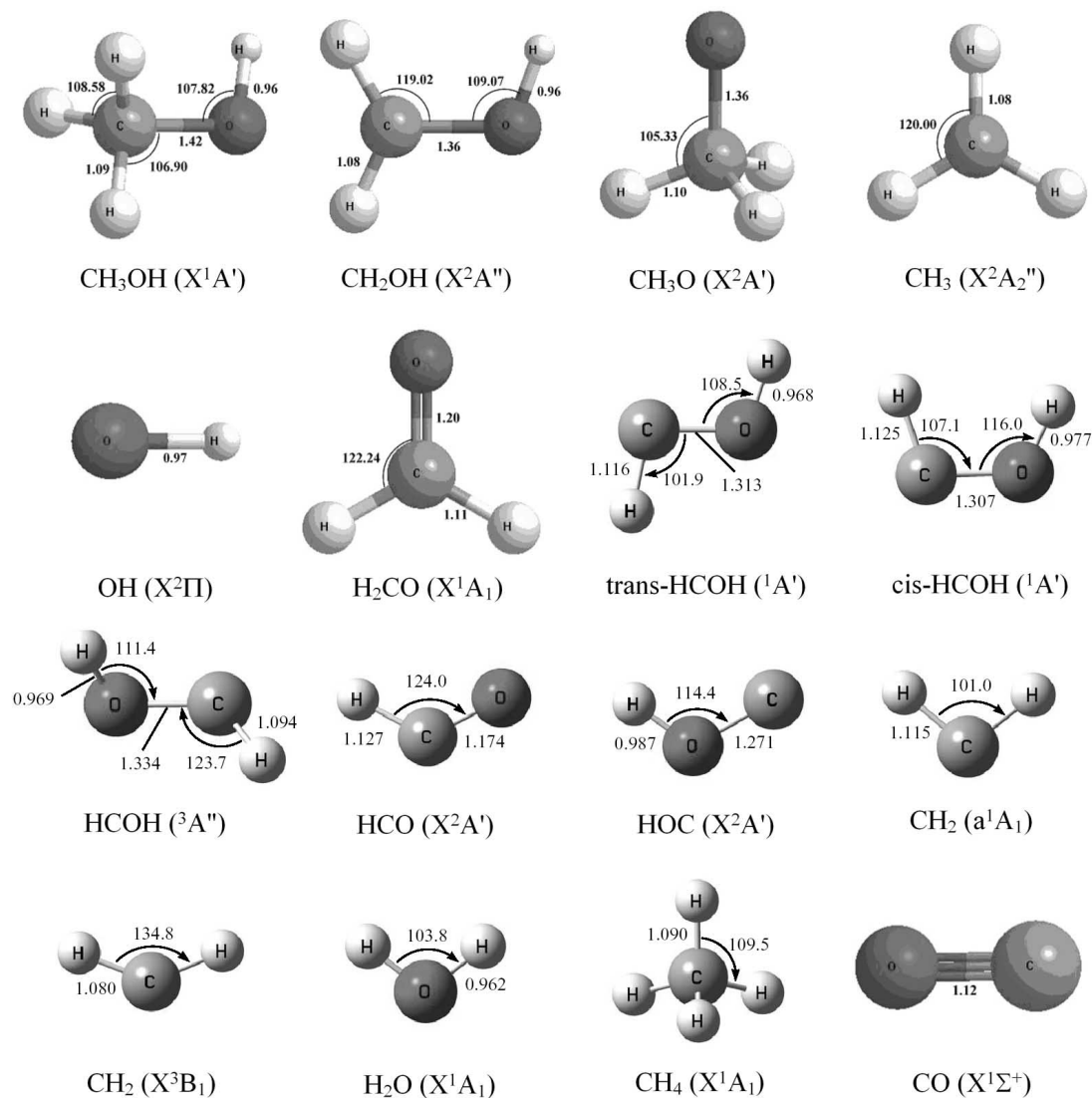


FIG. 2.—B3LYP/6-311G(d,p) optimized structures of molecules expected to form from the breakdown of methanol covered by the theoretical calculations in this study.

structures, vibrational frequencies, and infrared intensities. The energies were then refined by using the coupled cluster CCSD(T) method (Purvis & Bartlett 1982; Raghavachari et al. 1989) with the aug-cc-pVTZ basis functions (Dunning 1989) including the B3LYP/6-311G(d,p) zero-point energy corrections at the B3LYP/6-311G(d,p) optimized geometries. All calculations were carried out with the GAUSSIAN 98 program package (Frisch et al. 2001). At this level of theory, the calculated intensities are typically accurate to about 20% compared to gas-phase values (Galabov et al. 2002); however, experimentally derived solid-state intensities are used where possible.

4. RESULTS

4.1. Infrared Spectroscopy: Qualitative Analysis

Figure 1 shows the pristine methanol ice at 11 K, as well as after it was subjected to irradiation from 5 keV electrons at 100 nA for 1 hr. Figures 4a and 4b highlight the differences between the methanol ice at 11 K before irradiation, after irradiation, and after it has been warmed to 113 K within the spectral regions 2500–1500 cm^{-1} and 1500–500 cm^{-1} . We now describe the new absorp-

tion features as a result of irradiation first with comparison to other experiments, and then those observed during the subsequent warm-up of our sample up to 273 K. A list of the observed species can be found in Table 2.

The hydroxymethyl radical, $\text{CH}_2\text{OH}(X^2A'')$, was identified via its ν_4 (CO-stretching) fundamental at 1192 cm^{-1} , which is in agreement with previous studies that have identified the radical either in matrix isolation studies at 1183 cm^{-1} (Jacox 1981), or at 1197 cm^{-1} in UV irradiation experiments (Gerakines et al. 1996). Note that we were unable to unambiguously confirm the presence of the ν_5 (CH_2 , OH-rocking) 1352 cm^{-1} band also reported by Gerakines et al. (1996), which our calculations estimate to be half as strong. Note that this feature was also identified in irradiation experiments carried out by Hudson & Moore (2000) at 1353 cm^{-1} , but reassigned tentatively to the absorption to the formate ion (HCOO^-).

We were unable to directly confirm the generation of the methoxy radical, $\text{CH}_3\text{O}(X^2A')$, due to the fact that most of the absorptions overlap with either methanol or other species covered in this study. Our calculations indicate that the strongest absorption, the ν_1 (CO-stretching) fundamental should be the easiest to

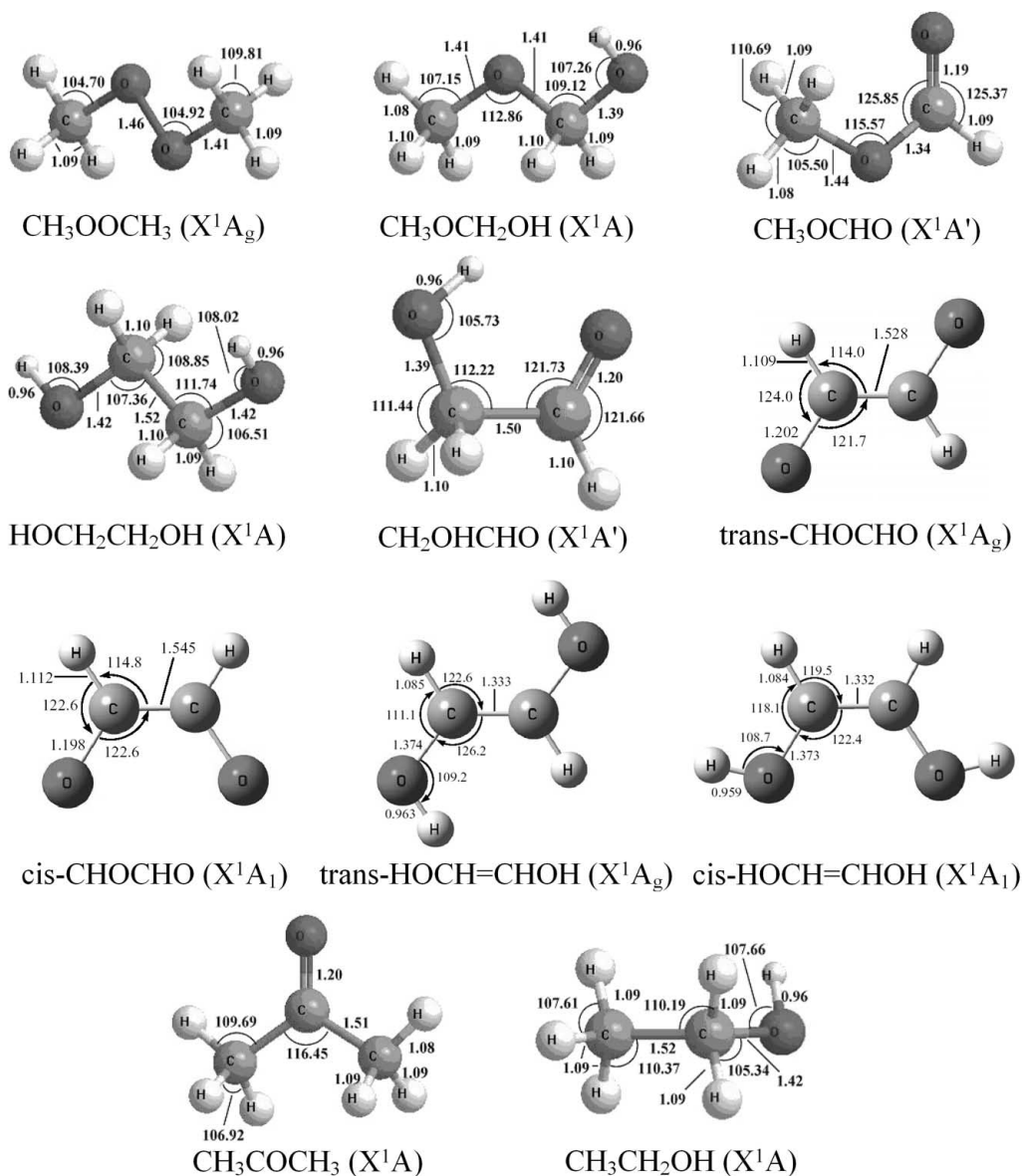


FIG. 3.—B3LYP/6-311G(d,p) optimized structures of molecules we expect to observe as products of radical-radical recombination, along with the structures of other molecules that may form.

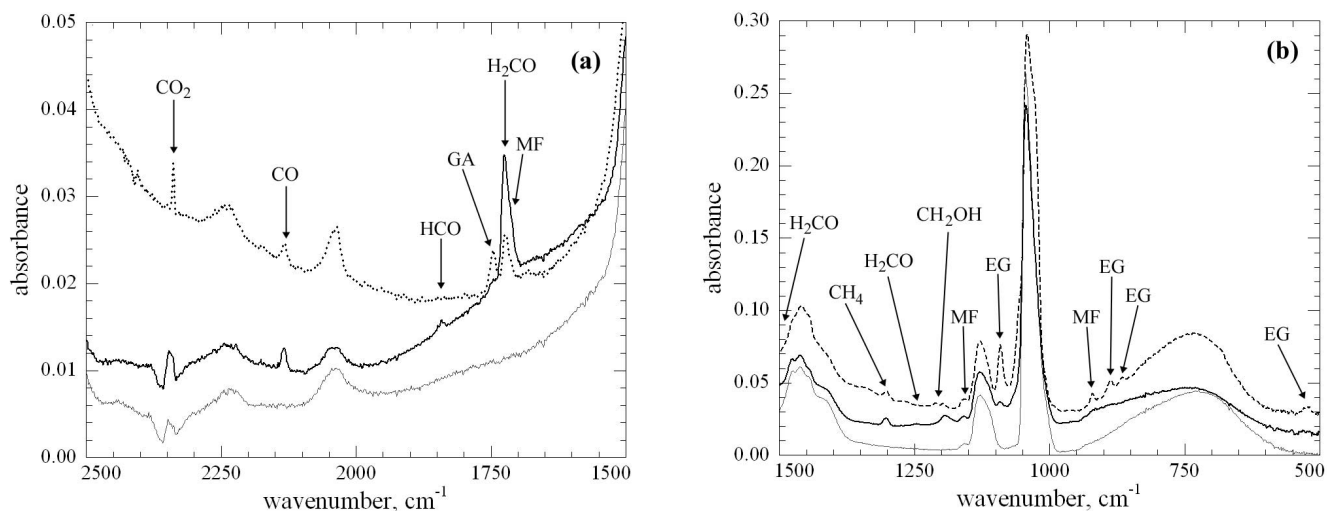


FIG. 4.—Comparison of the infrared spectra of the methane frost at 11 K before irradiation (*gray line*), after irradiation (*solid black line*), and during the warm-up process at 113 K (*dashed line*) highlighting regions between (a) 2500–1500 cm^{-1} and (b) 1500–500 cm^{-1} . The characterizations are given in Table 2. GA: glycolaldehyde, MF: methyl formate, EG: ethylene glycol.

TABLE 2
OBSERVED PEAK POSITIONS, ASSIGNMENTS, AND CHARACTERIZATIONS AFTER 1 hr OF IRRADIATION VIA 5 keV ELECTRONS AT 0.1 μ A,
TOGETHER WITH COMPARISONS FROM PREVIOUS STUDIES AND THEIR ASSIGNMENTS

Assignment	Present Work Band Position (cm^{-1})	Gerakines et al. (1996)	Hudson & Moore (2000)	Palumbo et al. (1999)
ν_4 CH ₂ OH.....	1192	1197		
ν_5 CH ₂ OH/ ν_2 HCOO ⁻ ?.....		1352	1353	
ν_4 H ₂ CO.....	1726	1719	1712	1720 ^b
ν_3 H ₂ CO.....	1496	1497	1499	
ν_2 H ₂ CO.....	1245	1244	1248	
ν_2 HCO.....	1849,1841	1850, 1863	1848	
ν_1 CO.....	2134	2138	2135	2136
ν_1 CO (¹³ C).....		2092		
ν_3 CO ₂	2345	2342	2341	2344
ν_3 CO ₂ (¹³ C).....		2278		
ν_2 CO ₂		655	654	660
ν_4 CH ₄	1303	1304	1303	1305
ν_3 CH ₄		3011		
ν_{14} CH ₃ OCHO.....	1718	1718		
ν_8 CH ₃ OCHO.....	1160 ^a	1160		
ν_5 CH ₃ OCHO.....	916 ^a	910		
ν_9 HOCH ₂ CH ₂ OH.....	1090	1088 ^c	1088	
ν_7 HOCH ₂ CH ₂ OH.....	889 ^a		885	
ν_6 HOCH ₂ CH ₂ OH.....	865 ^a		861	
ν_5 HOCH ₂ CH ₂ OH.....	525 ^a		524	
ν_{14} HCOCH ₂ OH.....	1747			
ν_1 H ₂ ?.....		4140		
ν_2 HCOO ⁻ ?.....			1384	
ν_5 HCOO ⁻ ?.....			1589	
ν_2 H ₂ O.....				1655

^a Visible only during warm-up.

^b Authors note band could also have contributions from acetone.

^c Assigned to "alcohols."

detect at around 694 cm^{-1} (Petraco et al. [2002] using the more accurate RCCSD(T)/TZ2P(f,d) level of theory indicate this absorption may occur closer to 745 cm^{-1}). RAIRS studies of the methoxy radical chemisorbed on copper surfaces show this intense band absorbs closer to 998 cm^{-1} (Andersson et al. 2002), which was hidden by the methanol absorptions occurring in this region. However, a weaker band at 1940 cm^{-1} ($2\nu_1$ overtone) might become detectable at higher concentrations.

Formaldehyde, H₂CO(X^1A_1), could be identified via three of its fundamentals: the ν_2 (CH₂ rocking) at 1245 cm^{-1} , ν_3 (CH₂ scissoring) at 1496 cm^{-1} , and ν_4 (CO stretching + CH₂ scissoring) at 1726 cm^{-1} . These bands were also identified by Gerakines et al. (1996) at 1244, 1497, and 1719 cm^{-1} as well as by Hudson & Moore (2000) at 1248, 1499, and 1712 cm^{-1} . Palumbo et al. (1999) also observed a band at 1720 cm^{-1} but admitted that there could be other species, such as acetone, contributing to this feature. These absorptions are found to be in good agreement with polycrystalline formaldehyde at 4 K, where they appear at 1250, 1494, and 1715 cm^{-1} (Harvey & Ogilvie 1962).

The presence of the formyl radical, HCO(X^2A'), was confirmed via its fundamental ν_2 (CO stretching) at 1842 cm^{-1} (found to consist of two underlying bands at 1849 and 1841 cm^{-1} in a 1:4 ratio). Because of its low abundance and overlap from methanol vibrations, the other bands were unlikely to be detected. Hudson & Moore (2000) report also identifying this molecule at 1848 cm^{-1} . Gerakines et al. (1996) also report two different band positions for this absorption, at 1850 and 1863 cm^{-1} , and conclude the molecule is formed in two different matrix sites.

The fundamental of carbon monoxide, CO($X^1\Sigma^+$), could be found at 2134 cm^{-1} , in accordance with previous experiments from Gerakines et al. (1996) at 2138 cm^{-1} , Palumbo et al. (1999) at 2136 cm^{-1} , and Hudson & Moore (2000) at 2135 cm^{-1} . This band position is found to be in accordance with carbon monoxide in several different matrices, such as in an oxygen matrix at 2136 cm^{-1} (Sandford et al. 1988).

Weak absorptions arising from the fundamental ν_3 (asymmetric stretch) of carbon dioxide, CO₂($X^1\Sigma_g^+$), could be found at 2345 cm^{-1} . Gerakines et al. (1996) found absorptions at 2342 cm^{-1} (as well as from the ¹³C isotope at 2278 cm^{-1}) and from the ν_2 (out-of-plane bend) at 650 cm^{-1} . Palumbo et al. (1999) found corresponding absorptions at 2344 and 660 cm^{-1} , respectively. Hudson & Moore (2000) also reported the molecule appearing at 2341 and 654 cm^{-1} . These band positions conform to those of carbon dioxide in different matrix sites, for example, in oxygen matrices at 2342 and 662 cm^{-1} (Sandford & Allamandola 1990).

Methane, CH₄(X^1A_1), could clearly be identified via absorption from the fundamental ν_4 (deformation) at 1303 cm^{-1} . This absorption was also observed by Hudson & Moore (2000) at the same frequency. This value is also in agreement with experiments from Gerakines et al. (1996), which found the methane molecule at 1304 cm^{-1} , and also at 3011 cm^{-1} , due to the absorptions from the ν_3 (degenerate stretch) fundamental. Palumbo et al. (1999) report the same findings at 1305 and 3010 cm^{-1} , respectively. The presence of the ν_3 fundamental could not be fully established. In argon matrices, these absorptions are found to occur at 1304 and 3025 cm^{-1} (Govender & Ford 2000).

It is of note that although the following molecules were searched for, they could not be identified unambiguously in the present set of experiments. These include the hydroxyl radical, $\text{OH}(X^2\Pi)$, from which the fundamental absorption may overlap with methanol, which has been experimentally determined in matrix isolated experiments to absorb at 3548 cm^{-1} (Cheng et al. 1988). The methyl radical, $\text{CH}_3(X^2A_2')$, could also not be unambiguously identified in these experiments, seen easiest by its ν_1 (CH_3 wagging) fundamental, which absorbs in, for example, nitrogen matrices at 611 cm^{-1} (Milligan & Jacox 1967).

No evidence was found for the presence of water, $\text{H}_2\text{O}(X^1A_1)$, in these experiments, in contrast to experiments by Palumbo et al. (1999), who report absorptions arising from the ν_2 (bending) fundamental at 1655 cm^{-1} . Matrix isolation studies, for example, in nitrogen find this band to absorb at 1598 cm^{-1} (Fredin et al. 1977).

Both *cis* and *trans* isomers of hydroxymethylene, $\text{HCOH}(X^1A')$, were searched for, but as most of the absorptions underlie stronger absorptions from methanol, identification of this species would be difficult.

The band appearing at 1091 cm^{-1} was initially assigned to "alcohols" by Gerakines et al. (1996); Moore et al. (1996) claimed that this absorption was exclusively from ethanol, $\text{C}_2\text{H}_5\text{OH}(X^1A)$. However, our calculations show that the ν_8 fundamental of ethanol that would be responsible for this absorption is one of the least intense and is therefore unlikely.

Regarding the presence of acetone, $\text{CH}_3\text{COCH}_3(X^1A_1)$, whose presence has been postulated by both Baratta et al. (1994) from bands appearing at 1720 , 1444 , 1232 , and 1090 cm^{-1} , and also by Moore et al. (1996) for a feature occurring around 532 – 516 cm^{-1} . However, our calculations indicate that again, more intense bands should be visible if this molecule is present, in particular, the ν_{11} fundamental at 1193 cm^{-1} and the ν_{13} fundamental at 1344 cm^{-1} .

Hudson & Moore (2000) also claim to have identified the formate ion, HCOO^- , based on absorptions at 1589 , 1384 , and 1353 cm^{-1} . None of these absorption features could be found in our experiment, and these assignments are in disagreement with both matrix isolation and calculated frequencies (Forney et al. 2003).

As our previous work on the irradiation of methane and methane mixed with carbon monoxide has shown, radicals formed within the matrix can recombine with neighboring radicals to form new species both during the irradiation period and on warm-up of the ice when these radicals become mobile (Bennett et al. 2005, 2006). In the case of methane, methyl radicals, $\text{CH}_3(X^2A_2')$, generated recombined to form ethane, $\text{C}_2\text{H}_6(X^1A_{1g})$. In the case of methane mixed with carbon monoxide, the hydrogen atom left over from the production of the methyl radical initially reacted with carbon monoxide to produce the formyl radical, $\text{HCO}(X^2A')$, which could then subsequently recombine with the methyl radical to produce acetaldehyde, $\text{CH}_3\text{CHO}(X^1A')$. We therefore also searched for the species thought to form via recombination of important radical reactions as shown in Figure 5.

Gerakines et al. (1996) also claimed that the bands at 910 , 1160 , and 1718 cm^{-1} were due to the presence of methyl formate, $\text{CH}_3\text{OCHO}(X^1A')$. In our experiments, the band at 1718 cm^{-1} could be identified as the ν_{14} fundamental from methyl formate. The ν_5 and ν_8 fundamentals, however, can only clearly be seen in the warm-up procedure at 1160 and 916 cm^{-1} , respectively.

Hudson & Moore (2000) were able to identify ethylene glycol, $\text{HOCH}_2\text{CH}_2\text{OH}(X^1A)$, from absorptions appearing at 1088 , 1046 , 885 , 861 , and 524 cm^{-1} . In our experiments, we were also able to identify these peaks at $1090(\nu_9)$, $889(\nu_7)$, $865(\nu_6)$, and $525(\nu_4)\text{ cm}^{-1}$; however, only the ν_9 fundamental is visible during the irradiation period, with the rest only becoming visible during warm-up (Fig. 6).

Glycolaldehyde, $\text{CH}_2\text{OHCHO}(X^1A')$, could only be identified by its ν_{14} fundamental at 1747 cm^{-1} . This is in good agreement with previous matrix isolation studies of glycolaldehyde in an Argon matrix at 13 K where it can be seen at 1747 cm^{-1} (Aspiala et al. 1986). We also find that a second band at 1705 cm^{-1} was not identified. This band has been disputed previously over whether or not it is assigned to a second matrix site of glycolaldehyde, or the keto-enol tautomer ethene-1,2-diol, which can be found as either the *trans*- $\text{HOCH}=\text{CHOH}(X^1A_g)$ or *cis*- $\text{HOCH}=\text{CHOH}(X^1A_i)$ isomer. Although the second of these does have an infrared active absorption in this region, the DFT calculations show that there should be several more intense bands observable if this molecule is present. Thus, it seems more likely that where this second band is seen it originates from a second matrix site as concluded by Yeom & Frei (2003).

None of the other species speculated to form via the recombination of radicals as listed in Table 4 could be detected unambiguously in our experiments.

4.2. Quantitative Analysis

The temporal development of the column density of methanol was traced by fitting Gaussians to the ν_8 (CO stretching) and ν_{11} (CH_2 rocking) bands, which combined have been determined to have a band strength of $1.3 \times 10^{-17}\text{ cm molecule}^{-1}$ (Palumbo et al. 1999). Using this value, the column density of methanol prior to irradiation was found to be $(1.64 \pm 0.04) \times 10^{17}\text{ molecules cm}^{-2}$. After 1 hr of exposure to 5 keV electrons at a beam current of 100 nA , the column density was found to be $(1.39 \pm 0.02) \times 10^{17}\text{ molecules cm}^{-2}$, indicating that $(2.44 \pm 0.43) \times 10^{16}\text{ molecules cm}^{-2}$ of methanol were destroyed during irradiation. Recalling from § 2 that the number of electrons hitting the sample is $5.9 \times 10^{14}\text{ electrons cm}^{-2}$, we can estimate that each electron destroys 41 ± 7 molecules of methanol. During the warm-up period, the column density of methanol remains unchanged (within error limits), and an increase in the abundance is seen around 108 – 124 K , which is assumed to be accounted for by a change in the absorption coefficient during transformation into the α -phase. The methanol sublimates quickly starting at 141 K , with no traces of methanol being present by 152 K .

For the hydroxymethyl radical, the ν_4 (stretch) at 1192 cm^{-1} was used to follow the column density using a calculated A value of $1.6 \times 10^{-17}\text{ cm molecule}^{-1}$. This gives a column density after irradiation of $(5.02 \pm 0.17) \times 10^{15}\text{ molecules cm}^{-2}$. Taking into account the number of electrons, we can conclude that each electron generated 8.5 ± 0.3 molecules of the hydroxymethyl radical. The column density of the hydroxymethyl radical remains constant until the heating program is initiated, after which around 25 K it increases steadily up to a maximum at 49 K , after which the column density begins to fall rapidly until about 103 K , where it remains constant (could be due to underlying absorptions from another molecule). Here, it remains constant until about 160 K when it begins to sublime, with no trace left after 178 K .

Considering the column density of formaldehyde, the ν_4 band at 1726 cm^{-1} was used, with a calculated A value of $1.8 \times 10^{-17}\text{ cm molecule}^{-1}$. Here, the column density after irradiation was found to be $(1.39 \pm 0.12) \times 10^{15}\text{ molecules cm}^{-2}$, or 2.4 ± 0.2 per electron. The column density remains the same after the irradiation period and until the warm-up reaches 63 K , after which it decreases steadily until 108 K . Possibly, the phase transformation of the methanol lattice causes a slight increase in its abundance until around 118 K , after which it again decreases rapidly, undetectable at 131 K .

The column density of the formyl radical was traced through the 1842 cm^{-1} (ν_2) mode, employing a calculated A value of

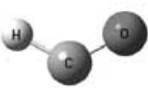
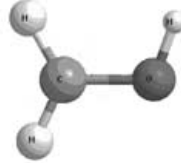
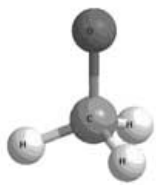
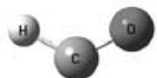
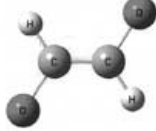
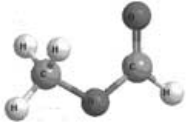
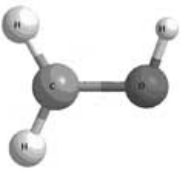
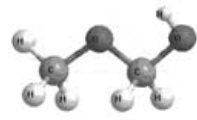
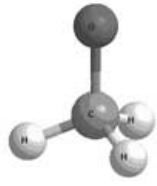
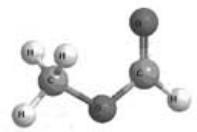
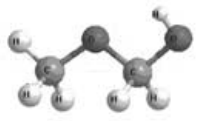
Radical 1 Radical 2	 HCO	 CH₂OH	 CH₃O
 HCO	 CHOCHO	 HOCH₂CHO	 CH₃OCHO
 CH₂OH	 HOCH₂CHO	 HOCH₂CH₂OH	 CH₃OCH₂OH
 CH₃O	 CH₃OCHO	 CH₃OCH₂OH	 CH₃OOCH₃

FIG. 5.—Species expected to be produced via radical-radical recombination reactions from those radicals previously identified or assumed to be present during the irradiation of pure methanol ices. Species detected in this experiment are highlighted in bold.

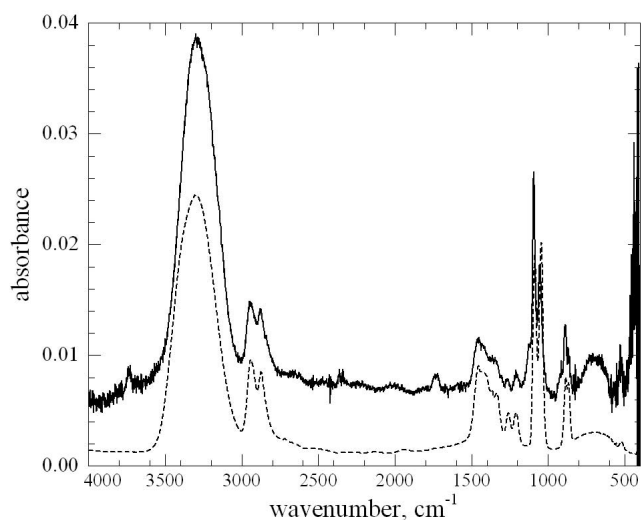


FIG. 6.—Infrared spectra of the residue from irradiated methanol after warming to 173 K (solid line). For comparison, the spectra of pure ethylene glycol obtained from R. L. Hudson et al. (2006, private communication) is overlaid (dashed line).

1.5×10^{-17} cm molecule⁻¹. The column density after irradiation was found to be $(2.26 \pm 0.42) \times 10^{14}$ molecules cm⁻², or 0.4 ± 0.1 per electron. The column density of the formyl radical appears to decrease again at around 25 K, disappearing (within error limits) by 105 K.

The column density of carbon monoxide was traced through the ν_1 (CO stretch) at 2134 cm⁻¹ using an A value of 1.1×10^{-17} cm molecule⁻¹ (Gerakines et al. 1995). The column density after irradiation was found to be $(7.24 \pm 0.38) \times 10^{14}$ molecules cm⁻², or 1.2 ± 0.1 per electron. The column density of carbon monoxide does appear to increase slightly during the initial stages of the warm-up to about 69 K, but then begins to decrease rapidly between 110 K and 122 K, by which time there is no sign of this molecule left.

For methane, the ν_4 band at 1303 cm⁻¹ was used to derive the column density using an A value of 7.0×10^{-18} cm molecule⁻¹ (Kerkhoff et al. 1999). The column density after irradiation was found to be $(2.80 \pm 0.08) \times 10^{15}$ molecules cm⁻², or 4.7 ± 0.1 per electron. For methane, the column density remains constant until around 49 K, after which it begins to decrease slowly until 114 K, where it sublimates rapidly, being undetectable within error limits by 122 K.

For several of the other species, it is possible only to derive upper limits for their column densities after irradiation. For carbon

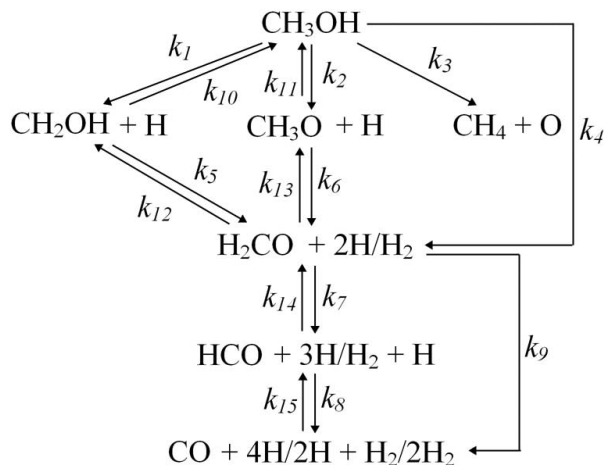


FIG. 7.—Reaction scheme used to fit the column densities of the products observed during irradiation (excluding glycolaldehyde, methyl formate, and ethyl glycol).

dioxide, $\text{CO}_2(X^1\Sigma_g^+)$, using the 2342 cm^{-1} band (ν_3) with an A value of $7.6 \times 10^{-17}\text{ cm molecule}^{-1}$ (Yamada & Person 1964) we found an upper limit of $(1.51 \pm 0.75) \times 10^{14}\text{ molecules cm}^{-2}$, or 0.26 ± 0.13 per electron. The amount of carbon dioxide present seems to decrease on warm-up, subliming rapidly at 114 K, with no trace left by 122 K.

For glycolaldehyde, we used its ν_{14} band at 1747 cm^{-1} and an A value of $2.6 \times 10^{-17}\text{ cm molecule}^{-1}$ (Hudson et al. 2005) to derive an upper value of $(1.8 \pm 0.3) \times 10^{14}\text{ molecules cm}^{-2}$, or 0.30 ± 0.05 per electron. During warm-up, the column density increases slightly after around 25 K, rising sharply with the onset of the phase change, and reaching a maximum value of $(8.61 \pm 0.8) \times 10^{14}\text{ molecules cm}^{-2}$ by 116 K. The column density falls steadily, completely sublimating at 193 K.

An upper limit for the column density of methyl formate of $(1.3 \pm 0.5) \times 10^{15}\text{ molecules cm}^{-2}$ was found by using the ν_5 (CO stretch) band at 916 cm^{-1} using a calculated A value of $4.0 \times 10^{-18}\text{ cm molecule}^{-1}$. This would correspond to 2.2 ± 0.9 produced per electron. During the warm-up period, a maximum column density of $(4.05 \pm 0.70) \times 10^{15}\text{ molecules cm}^{-2}$ was found at 113 K. From this point, the column density drops sharply but steadies out at 133 K. It then sublimates around 164–176 K.

For ethylene glycol, using an A value of $3.65 \times 10^{-18}\text{ cm molecules}^{-1}$ (calculated from relative areas and using the value from Hudson et al. [2005]) for the band appearing at 1090 cm^{-1} (ν_9) gives an upper limit of $(8.0 \pm 0.2) \times 10^{15}\text{ molecules cm}^{-2}$ at the end of irradiation (13.6 ± 0.3 per electron), which increases on warm-up to 113 K to a value of $(3.21 \pm 0.50) \times 10^{16}\text{ molecules cm}^{-2}$. The column density steadily declines until about 193 K, where it begins to sublime rapidly, with no trace left after 211 K. Figure 6 shows a comparison of the residue at 173 K compared to the spectra of pure ethylene glycol (obtained from R. Hudson) showing that the residue at this temperature is almost exclusively this molecule.

5. DISCUSSION

5.1. Reaction Scheme

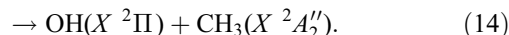
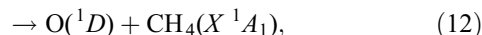
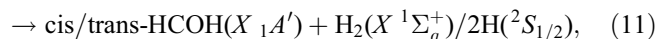
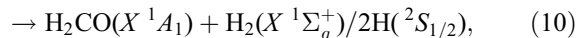
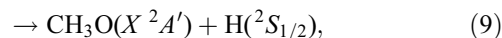
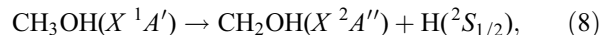
We now attempt to fit the column densities of the species produced by irradiation of the sample with a kinetic model. The reaction scheme is shown in Figure 7; the resulting system of coupled differential equations was solved numerically (Frenklach

TABLE 3
RATE CONSTANTS DERIVED VIA ITERATIVE SOLUTION
TO THE REACTION SCHEME DEPICTED IN FIG. 6

Reaction	Rate Constant
$\text{CH}_3\text{OH} \rightarrow \text{CH}_2\text{OH} + \text{H}$	$k_1 = 6.95 \times 10^{-5}$
$\text{CH}_3\text{OH} \rightarrow \text{CH}_3\text{O} + \text{H}$	$k_2 = 1.04 \times 10^{-4}$
$\text{CH}_3\text{OH} \rightarrow \text{CH}_4 + \text{O}$	$k_3 = 6.15 \times 10^{-6}$
$\text{CH}_3\text{OH} \rightarrow \text{H}_2\text{CO} + 2\text{H}/\text{H}_2$	$k_4 = 5.09 \times 10^{-6}$
$\text{CH}_2\text{OH} \rightarrow \text{H}_2\text{CO} + \text{H}$	$k_5 = 2.55 \times 10^{-6}$
$\text{CH}_3\text{O} \rightarrow \text{H}_2\text{CO} + \text{H}$	$k_6 = 7.59 \times 10^{-5}$
$\text{H}_2\text{CO} \rightarrow \text{HCO} + \text{H}$	$k_7 = 4.40 \times 10^{-4}$
$\text{HCO} \rightarrow \text{CO} + \text{H}$	$k_8 = 6.04 \times 10^{-9}$
$\text{H}_2\text{CO} \rightarrow \text{CO} + 2\text{H}/\text{H}_2$	$k_9 = 4.62 \times 10^{-4}$
$\text{CH}_2\text{OH} + \text{H} \rightarrow \text{CH}_3\text{OH}$	$k_{10} = 8.17 \times 10^{-20}$
$\text{CH}_3\text{O} + \text{H} \rightarrow \text{CH}_3\text{OH}$	$k_{11} = 5.61 \times 10^{-20}$
$\text{H}_2\text{CO} + \text{H} \rightarrow \text{CH}_2\text{OH}$	$k_{12} = 7.04 \times 10^{-23}$
$\text{H}_2\text{CO} + \text{H} \rightarrow \text{CH}_3\text{O}$	$k_{13} = 1.07 \times 10^{-22}$
$\text{HCO} + \text{H} \rightarrow \text{H}_2\text{CO}$	$k_{14} = 2.57 \times 10^{-19}$
$\text{CO} + \text{H} \rightarrow \text{HCO}$	$k_{15} = 3.79 \times 10^{-20}$

NOTE.—Units are s^{-1} (unimolecular decomposition; k_1 – k_9) and $\text{cm}^2\text{ s}^{-1}$ (bimolecular reactions; k_{10} – k_{15}).

et al. 1992). The underlying rate constants found for each process are compiled in Table 3, and the resulting kinetic fits to the column densities of each species are shown in Figure 8 (note that as we were unable to produce the temporal development of the column density of the methoxy radical, only the fitted results from our scheme are presented). Note that the scheme does not cover the observed products assumed to be produced via radical-radical recombination reactions in the warm-up phase. Considering first the initial radiolysis-induced decomposition of methanol, different pathways are feasible:



However, as we were only able to identify products from reactions (8), (10), and (12), only these reactions were included in our reaction scheme. In addition, reaction (9) is proposed to be present based on the identification of methyl formate, which, if we assume it is generated by the recombination of radicals, requires a production pathway for the methoxy radical. The rate constants for reactions (8), (9), and (12) and reaction (10) were found to be $k_1 = 6.95 \times 10^{-5}$, $k_2 = 1.04 \times 10^{-4}$, $k_3 = 6.15 \times 10^{-6}$, and $k_4 = 5.09 \times 10^{-6}\text{ s}^{-1}$, respectively. Theoretical calculations on the CH_4O potential energy surface at the CCSD(T)/6-311+G(3df,2p) level of theory carried out by Chang & Lin (2004) suggest that the energy needed to be overcome for these reactions are 4.03, 4.36, 5.86, and 3.94 eV, respectively. Thus, the lower reaction rate found for the generation of methane and an oxygen atom (reaction [12]) could be explained by the higher energy to be overcome. The low reaction rate of reaction (10),

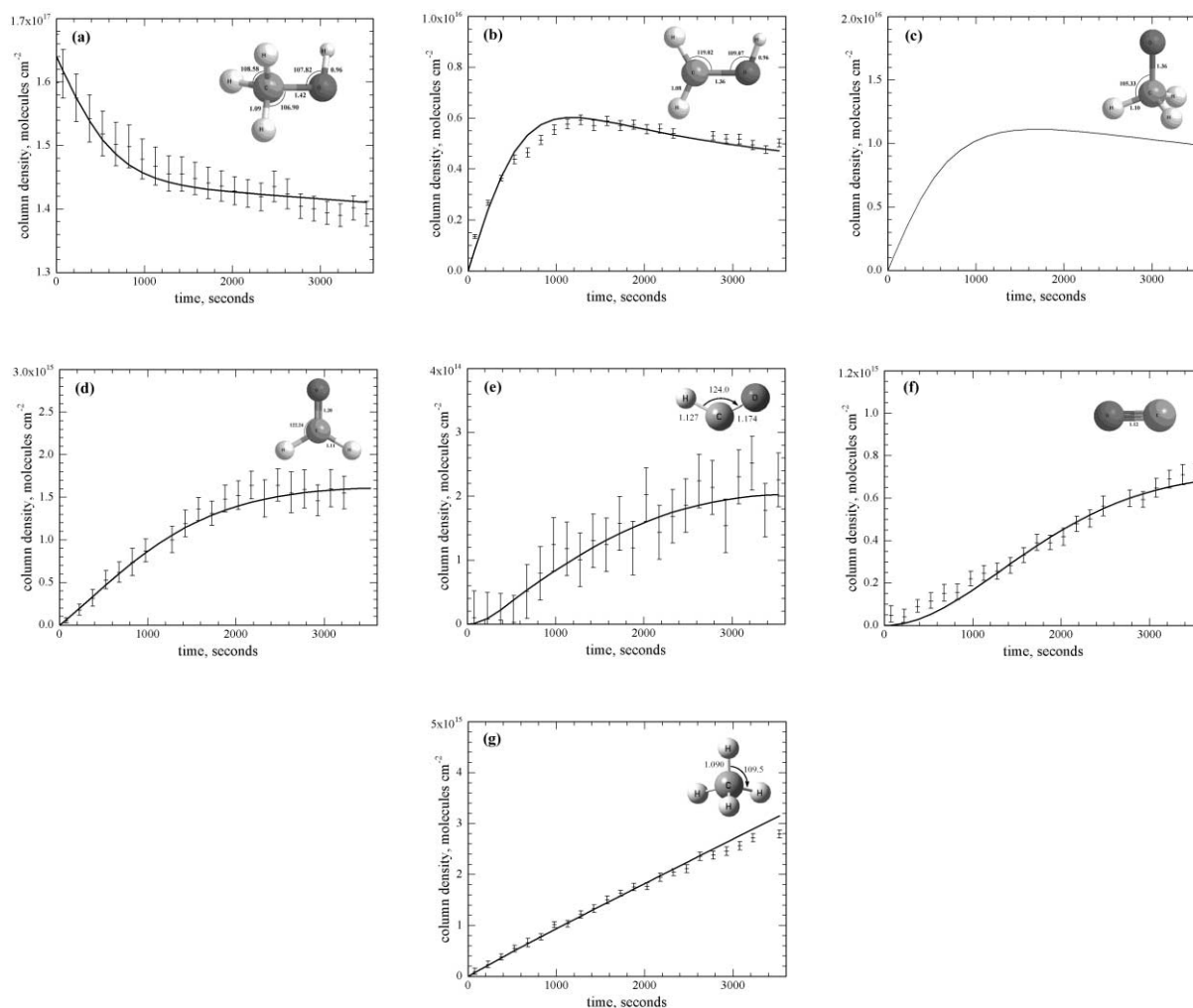
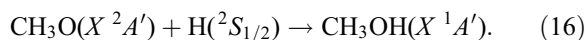
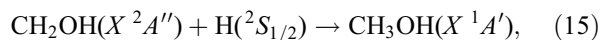


FIG. 8.—Fit of column densities of (a) methanol, (b) hydroxymethyl, (c) methoxy (fit only), (d) formaldehyde, (e) formyl, (f) carbon monoxide, and (g) methane.

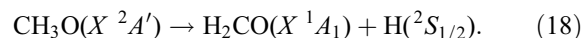
i.e., the formation of formaldehyde and molecular hydrogen, is low despite this pathway having a lower energy to overcome. Reactions leading to the generation of the hydroxymethyl (reaction [8]) and methoxy (reaction [9]) radicals and atomic hydrogen via the unimolecular decomposition of methanol and a simple atomic hydrogen loss appear to be the dominant pathways. Note that k_1 may be underestimated in this current model as pathways to form ethylene glycol were omitted from the model. As the radiolysis proceeds, more hydrogen atoms are available in the matrix, and the possibility for them to react with the previously formed radicals via reactions (8) and (9) to reform methanol increases; these reactions were also included in the model,



The rate constants for reactions (15) and (16) were found to be of the same order, $k_{10} = 8.17 \times 10^{-20}$ and $k_{11} = 5.61 \times 10^{-20}$ $\text{cm}^2 \text{molecule}^{-1} \text{s}^{-1}$, suggesting the presence of a barrierless atom-radical recombination reaction.

Considering next the production of formaldehyde, we have already considered its formation from methanol (reaction [10]) but

would now also like to consider the two following pathways via unimolecular decomposition by atomic hydrogen loss,



Here, the rate constants were found to be $k_5 = 2.55 \times 10^{-6}$ and $k_6 = 7.59 \times 10^{-5} \text{ s}^{-1}$; the calculated energies are 2.80 and 1.85 eV, respectively. This indicates that it is easier to produce formaldehyde through the methoxy intermediate (CH_3O) than through the hydroxymethyl radical (CH_2OH); this pathway contributes to the formation of formaldehyde in addition to the one-step route from the unimolecular decomposition of methanol itself. For completeness, the back reactions were also included, where the rate constants of $k_{12} = 7.04 \times 10^{-23}$ and $k_{13} = 1.07 \times 10^{-22} \text{ cm}^2 \text{molecule}^{-1} \text{ s}^{-1}$. Note that these reactions are found to occur much slower than the hydrogen additions to the open shell species (reactions [15] and [16]), indicative that in this case an entrance barrier must be overcome for the reaction to proceed. The rates of these reactions reflect well from the calculated energy barriers that were reported as 0.50 eV and 0.22 eV, respectively.

TABLE 4
SUMMARY OF TEMPORAL CHANGES IN COLUMN DENSITY OF THE OBSERVED SPECIES BASED ON THE INDICATED BAND POSITION
AND THE CORRESPONDING A VALUE AT THE END OF IRRADIATION

Species	Band Position (cm^{-1})	A (cm molecule^{-1})	Change in Column Density over Irradiation (molecules cm^{-2})	Number of Molecules Produced per Electron ^a	Minimum Energy per Molecule (eV)	Total Energy Translated to Matrix per Electron (eV)	Sublimation Temperature (K)
CH ₃ OH.....	1031	1.3×10^{-17c}	$-(2.44 \pm 0.43) \times 10^{16}$	-41.3 ± 7.3	141–152 ^b
CH ₂ OH.....	1192	1.6×10^{-17d}	$(5.02 \pm 0.17) \times 10^{15}$	8.5 ± 0.3	4.03	34.28 ± 1.16	160–178
H ₂ CO.....	1726	1.8×10^{-18d}	$(1.39 \pm 0.12) \times 10^{15}$	2.4 ± 0.2	3.94	9.28 ± 0.80	118–131
HCO.....	1842	1.5×10^{-17d}	$(2.26 \pm 0.42) \times 10^{14}$	0.4 ± 0.1	8.06	3.08 ± 0.57	<105
CO.....	2134	1.1×10^{-17e}	$(7.24 \pm 0.38) \times 10^{14}$	1.2 ± 0.1	7.73	9.48 ± 0.50	110–122
CH ₄	1303	7.0×10^{-18f}	$(2.80 \pm 0.08) \times 10^{15}$	4.7 ± 0.1	5.86	27.76 ± 0.81	114–122

NOTES.—The temperature at which the species sublimated from the matrix is also indicated. The minimum energy required to produce one molecule of each species is listed in eV (values taken from Chang & Lin 2004; Zhang et al. 2004) combined with the total energy that must be translated to the matrix per impinging electron. Also listed is the number of carbon atoms within the reported column densities.

^a Based on 5.9×10^{14} electrons cm^{-2} hitting the target (see § 2).

^b Phase change to α at 108–124 K.

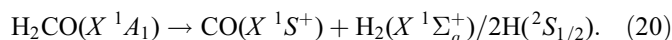
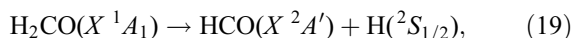
^c Value from Palumbo et al. (1999).

^d Calculated value (see Appendix).

^e Value from Gerakines et al. (1995).

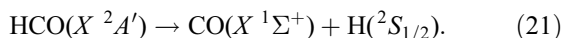
^f Value from Kerkhof et al. (1999).

The formaldehyde molecule can be further processed via reactions (19) and (20),



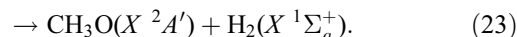
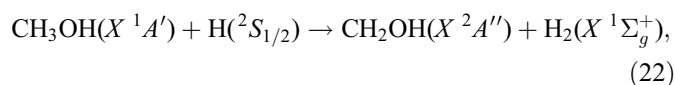
The rate constants for these reactions are found to be $k_7 = 4.40 \times 10^{-4}$ and $k_9 = 4.62 \times 10^{-4} \text{ s}^{-1}$, respectively. The relative energies are found to be 4.12 and 3.79 eV from a globally fitted CCSD(T)/aug-cc-pVTZ potential energy surface of CH₂O; note that the reaction rates and energy barriers are similar where the reaction proceeding quicker has the lower barrier (Zhang et al. 2004). The rate constants for the reverse of reaction (19) was found to be $k_{14} = 2.57 \times 10^{-19} \text{ cm}^2 \text{ molecule}^{-1} \text{ s}^{-1}$, once again demonstrating that the reaction of hydrogen with an open shell molecule proceeds faster.

The last pathway we investigated is the alternative mechanism on the formation of carbon monoxide via the unimolecular decomposition of the formyl (HCO) radical,



The reaction endoergicity for this reaction was calculated to be 0.73 eV using the CCSD(T)/aug-cc-pVTZ level of theory (Bennett et al. 2005). The rate of this reaction is $k_8 = 6.04 \times 10^{-9} \text{ s}^{-1}$, indicating that the predominant pathway to carbon monoxide formation is reaction (20), although this additional pathway is also significant. The reverse reaction, calculated to have a barrier of 0.12 eV, was found to have a rate constant of $k_{15} = 3.79 \times 10^{-20} \text{ cm}^2 \text{ molecule}^{-1} \text{ s}^{-1}$, slower than the hydrogen atom–radical recombination reactions as elucidated in the previous paragraphs.

The involvement of suprathermal hydrogen atom abstraction reactions generated primarily by reactions (8) and (9) cannot be ruled out, although they were not included in our reaction scheme. These reactions could be responsible for additional hydrogen abstraction reactions as follows:



Calculations at the G2 level of theory show that these reactions have barriers of only 0.39 and 0.61 eV (compared to 4.03 and 4.36 eV from reactions [8] and [9]), which may be overcome by the kinetic energy the suprathermal hydrogen atoms possess, and are exoergic due to the favorable formation of molecular hydrogen (Blowers et al. 1998). Indeed, hydrogen abstraction reactions by suprathermal reactions analogous to those for hydrogen elimination reactions can be found (e.g., Woon 2002).

5.2. Energetics

Table 4 summarizes the minimum energy required to be released from the impinging electron to the matrix to account for the observed species in this experiment, excluding carbon dioxide, glycolaldehyde, ethylene glycol, and methyl formate. As an example, the minimum energy to produce a molecule of carbon monoxide would be via the loss of molecular hydrogen from methanol (3.94 eV) followed by the loss of molecular hydrogen from formaldehyde (3.79 eV), giving 7.73 eV as listed in Table 4. To account for the observed column densities of these listed products requires 83.9 ± 1.8 eV (recall that the CASINO calculations tell us that 390 eV will be absorbed into our sample). So far, only 22% of the kinetic energy of the impinging electrons transferred to the matrix is used to “chemically modify” the methanol sample.

To account for the observed column densities of carbon dioxide, ethylene glycol, glycolaldehyde, and methyl formate, the radical–radical recombination reactions (24)–(27) are suggested to occur. Here, it should be stressed that the kinetic model and the experimental data suggest that HCO, CH₂OH, and CH₃O are the most important and abundant radical species involved in the chemical processing of the methanol sample (Fig. 7; Table 4),

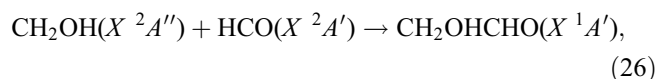
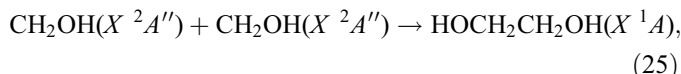
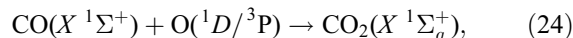


TABLE 5

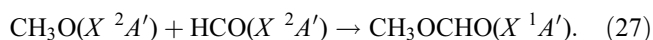
COMPARISON OF QUANTITATIVE RESULTS FROM ELECTRON BOMBARDMENT WITH 5 keV ELECTRONS AT 0.1 μA FOR 1 hr WITH THOSE FROM PREVIOUS EXPERIMENTS USING UV PHOTOLYSIS AND ION IRRADIATION

IRRADIATION SOURCE	DOSE (eV molecule ⁻¹)	[CH ₃ OH] DESTROYED		[CH ₄] (%)	[CH ₂ OH] (%)	[H ₂ CO] (%)	[HCO] (%)	[CO] (%)	[CO ₂] (%)	REF.
		$\times 10^{16}$	% of Amount Deposited							
5 keV electrons	1.4	2.4	15	11	21	6	1	3	0.6	1
UV photons.....	...	8.0	...	15	...	50	...	16	4	2
UV photons.....	7.2	31.0	89	9	...	3 ^a	1	43	10	3
UV photons.....	~80	18.4	92	6 ^a	...	7 ^a	...	44	14	4
3 keV He ⁺	60	150.0	98	5	...	9	...	7	6	5
30 keV protons	~156	19.5	98	1 ^a	...	2 ^a	...	25	6	4

NOTES.—The irradiation source is stated (refer to the individual papers for more details), the dose used, and the column density of methanol destroyed; the amount destroyed as a percentage of the amount deposited is also given. The column densities of the products identified in ours and other experiments are listed as a percentage of the column density of methanol reported destroyed.

^a Higher column densities were reported during the irradiation process than at the end.

REFERENCES.—(1) This work; (2) Allamondola et al. 1988, note 2: 1 composition (water : methanol); (3) Gerakines et al. 1996; (4) Baratta et al. 2002; (5) Baratta et al. 1994.



The energy required to produce one molecule of carbon dioxide via reaction (24) requires the formation of carbon monoxide (minimum of 7.73 eV) and an oxygen atom (5.86 eV), thus requiring a total of 13.59 eV molecule⁻¹. As before, taking into account the number of electrons and the column density of carbon dioxide observed at the end of the irradiation period, we can determine that 0.26 ± 0.13 molecules of carbon dioxide are formed per electron impact, requiring a total of 3.48 ± 1.73 eV. Similarly, the formation of ethylene glycol requires the combination of two hydroxymethyl radicals at 4.03 eV each, giving a total energy of 8.05 eV. To account for the observed number density, we can establish that 13.57 ± 0.34 molecules are produced per electron, therefore requiring an energy of 109.31 ± 2.73 eV per electron translated to the matrix. A similar approach is used to determine that to account for the column densities at the end of irradiation of glycolaldehyde and methyl formate requires 3.62 ± 0.62 and 26.72 ± 10.52 eV, respectively. The addition of these pathways brings the total energy used to chemically modify the methanol sample to 227.02 ± 11.17 eV per electron (58% of the energy). The remaining energy is released via phonon interaction to the matrix.

5.3. Carbon/Oxygen Budget

Here, we now briefly discuss the issue of whether or not the number of carbon/oxygen budget observed from the column densities of the identified products is able to account for the amount of carbon/oxygen atoms available as methanol decomposes. The reported number of carbon/oxygen atoms available corresponds to the change in column density of methanol during the irradiation period, i.e., $(2.44 \pm 0.43) \times 10^{16}$ molecules cm⁻². In the case of the number of carbon atoms contained in the products, we obtain a value of $(2.92 \pm 0.08) \times 10^{16}$ carbon atoms cm⁻². Similarly, for the oxygen atoms we determine there are $(2.69 \pm 0.08) \times 10^{16}$ oxygen atoms cm⁻². Therefore, within the error limits, the carbon and oxygen budgets are conserved.

5.4. Comparison to Previous Experiments

We now would like to compare quantitatively the results of electron bombardment on pure methanol ices with those from

experiments using UV photons and high-energy ions as the source of irradiation. Table 5 summarizes experiments where quantitative information regarding the destruction of methanol and production of new molecules was presented. The column densities of the species that could be produced directly from the decomposition of methanol (namely methane, the hydroxymethyl radical, and formaldehyde) are notably much smaller in each of the other experiments listed, with the possible exception of those by Allamondola et al. (1988). This is due to the fact that these experiments in general exposed the molecules to much larger irradiation doses and the initial products formed were subsequently destroyed (about 15% of our methanol was destroyed, compared to values between 89% and 96% as listed by other experiments). In the case of experiments by Allamondola et al. (1988), as a 2:1 water matrix was used, it is possible that additional reactions involving water are responsible for maintaining their high column densities, in particular, for formaldehyde. In experiments where high doses were used, it is clear that formaldehyde has indeed been further processed to produce carbon monoxide as indicated by the fact that higher column densities were reported earlier on during the irradiation process.

6. ASTROPHYSICAL IMPLICATIONS

The present study has demonstrated the effects of keV electrons on methanol ice, which is a key component identified within interstellar ices (Gibb et al. 2004). As these ices are bombarded by MeV particles, up to 99.99% of their kinetic energy can be transferred into the electronic systems of the target molecules with a similar LET (a few keV μm^{-1}) to that of the keV electrons used in our systems. In both cases, the electronic energy is used to generate secondary electrons that can have kinetic energies up to a few keV; these electrons further process the ices through similar electronic transfer processes. It is therefore expected that the species found to form during the irradiation of our methanol ices can be expected to be produced in these interstellar ices. These molecules can then be injected into the gas-phase as a YSO begins to form and the ices begin to sublime, resulting in additional formation pathways to these molecules to supplement gas-phase processes. The failure of purely gas-phase chemical models, which perpetually underestimate the abundances of complex chemical species, has led to the inclusion in several models of surface-grain processes. A recent example by Garrod & Herbst (2006) incorporates

the recombination of radical species on the surfaces of interstellar grains to produce these molecules. While the authors conclude that these processes may contribute to the production of these complex species, the recombination of radical species is a limited process that is found to only be efficient within a narrow temperature range (20–40 K), restricted by the mobility of the radicals on the surface and sublimation of necessary reactants. On the other hand, production of these species by radiolysis induced processes has no such temperature restrictions even at 10 K, without the diffusion of radicals; neighboring molecules can still react to produce complex species.

The formation of methanol is thought to occur through the successive hydrogenation of carbon monoxide on the surface of interstellar grains. Laboratory experiments studying the conversion of CO to H₂CO and H₂CO to CH₃OH via addition of atomic hydrogen at low temperatures are found to conflict one another; Shiraki et al. (2004) find that the conversion rate for CO to H₂CO is twice as fast as that for H₂CO to CH₃OH; however, Hiraoka et al. (2005) find that the rate for H₂CO to CH₃OH is about 1 order of magnitude faster than for CO to H₂CO. Although our reaction rates are dependant on our matrix composition, we find that the addition of hydrogen to carbon monoxide proceeds faster ($k_{15} = 3.79 \times 10^{-20} \text{ cm}^2 \text{ molecule}^{-1} \text{ s}^{-1}$) than the addition of hydrogen to formaldehyde ($k_{12} = 7.04 \times 10^{-23}/k_{13} = 1.07 \times 10^{-22} \text{ cm}^2 \text{ molecule}^{-1} \text{ s}^{-1}$) in accordance with the lower energy barrier required to overcome (0.12 eV vs. 0.50/0.22 eV). The observed abundance ratios of CH₃OH, H₂CO, and CO were recently modeled by Maret et al. (2005) for low-mass protostars, assuming that the relative reaction probability of hydrogen reacting with CO and H₂CO were equal. However, observations that the CH₃OH/H₂CO ratio increases in more processing environments is yet to be understood. Here, the dust temperature may be as high as 40 K, where methanol cannot be formed efficiently as hydrogen atoms will not stick to the grain surface (Gibb et al. 2004; Fuente et al. 2005). This may point to radiolysis induced synthesis of methanol within the grains as suggested in laboratory experiments of water ices mixed with carbon monoxide, or methane (Hudson & Moore 1999; Wada et al. 2006).

Comets are often thought to provide a record of the “pristine material” of the interstellar cloud (i.e., interstellar ices) from which our solar system was formed (Ehrenfreund et al. 2004). Indeed, looking at the abundance ratios of CO/H₂CO/CH₃OH relative to water in both comets (e.g., Comet 2002 C1 [Ikeya-Zhang] gives 4.7:0.62:2.5) and interstellar ices (~10:1:5) we can conclude that they are compositionally very similar (Disanti et al. 2002; Gibb et al. 2004). Both the detection of ethylene glycol

in comet C/1995 O1 (Hale-Bopp) as well as methyl formate in, for example, comets C/2002 T7 (Linear) and C/2001 Q4 (Neat) has been confirmed (Crovisier et al. 2004; Remijan et al. 2006). This evidence points toward the possibility that perhaps these molecules have been formed in interstellar ices prior to the formation of the solar system. If this is the case, it could help explain why such large discrepancies are found in the methanol abundance. For example, if the methanol absorption at 9.75 μm (1026 cm^{-1}) were to contain underlying absorption features from a strong absorption from ethylene glycol at 9.56 μm (1046 cm^{-1}), the reported column density for methanol may be exaggerated.

In summary, we have identified the most important unimolecular decomposition pathways of methanol by irradiation from 5 keV electrons at 11 K; these are the formation of (1) the hydroxymethyl radical and atomic hydrogen, (2) the methoxy radical plus atomic hydrogen, (3) formaldehyde and molecular hydrogen, and (4) the formation of methane and atomic oxygen. These can then be further decomposed to produce the formyl radical and carbon monoxide. We have also demonstrated that it is possible to form carbon dioxide, methyl formate, glycolaldehyde, and ethylene glycol via radical-radical recombination. In addition, the unimolecular decomposition of methanol into methane and atomic oxygen shows that the reverse reaction (oxygen addition into methane to form methanol) may also occur as predicted by theoretical studies (Chang & Lin 2004). From an astrobiological viewpoint, the formation of these complex species in interstellar ices leads to the possibility that these molecules may have been available to the early Earth as life either originated or began to flourish. Carbohydrates will have been instrumental in the development of life on Earth and have important roles in life as we know it today, as energy sources, structural molecules (e.g., cellulose), synthesis of amino acids (e.g., Weber 1998), as well as key components of ribonucleic and deoxyribonucleic acids.

This material is based on work supported by the National Aeronautics and Space Administration through the NASA Astrobiology Institute under Cooperative Agreement NNA 04-CC08A issued through the Office of Space Science. We would like to thank Reggie Hudson for providing us with reference spectra of ethylene glycol, glycolaldehyde, methyl formate, and acetic acid. We are also grateful to Ed Kawamura (University of Hawai'i at Manoa, Department of Chemistry) for his support. S. H. S., B. J. S., and A. H. H. C. would like to thank the National Science Council of Taiwan and National Center for High-Performance Computing of Taiwan for their support.

APPENDIX

In order to correctly identify and quantify the new species produced during our experiment via infrared spectroscopy, it is necessary to carry out theoretical electronic structure calculations to give us information about the band positions where these molecules will absorb in the infrared region (given in cm^{-1}) and how strong these absorptions should be (cm molecule^{-1}). Although some information already exists regarding some of these data (both theoretical and experimental), it is prudent to use frequencies and intensities all derived from the same level of theory to avoid unnecessary complications and errors that may arise from combining the assortment of information already available. The vibrational frequencies and infrared intensities shown here were calculated from structures obtained from using the hybrid density functional B3LYP method (Lee et al. 1988; Becke 1993) with the 6-311G(d,p) basis functions. A scaling factor of 0.97 that was used to account for anharmonicity is consistent for this level of theory. The accuracy of the infrared intensities is accurate within 20% to gas-phase values at this level of theory (Galabov et al. 2002).

TABLE A6
CALCULATED VIBRATIONAL FREQUENCIES AND INTEGRAL ABSORPTION COEFFICIENTS OF VARIOUS SPECIES EXPECTED
TO BE PRODUCED FROM THE IRRADIATION OF METHANOL

Bands	Characterization	Band Position (cm^{-1})	A (cm molecule^{-1})
$\text{CH}_3\text{OH}(X^1A')$			
$\nu_1 (a'')$	(CH_3, CO) rocking	319	2.04×10^{-17}
$\nu_2 (a')$	CO stretching	1021	1.94×10^{-17}
$\nu_3 (a')$	(CH_2, CO) scissoring	1053	3.56×10^{-19}
$\nu_4 (a'')$	CH_2 rocking	1133	6.56×10^{-20}
$\nu_5 (a')$	(CH, CO) rocking	1338	4.19×10^{-18}
$\nu_6 (a')$	CH_2 (rocking + scissoring)	1444	9.22×10^{-19}
$\nu_7 (a'')$	CH_3 wagging	1447	4.23×10^{-19}
$\nu_8 (a')$	CH_2 scissoring	1463	6.44×10^{-19}
$\nu_9 (a')$	CH_2 symmetric stretching	2885	1.09×10^{-17}
$\nu_{10} (a'')$	CH_2 asymmetric stretching	2925	1.37×10^{-17}
$\nu_{11} (a')$	CH symmetric stretching	3010	5.76×10^{-18}
$\nu_{12} (a')$	OH stretching	3723	3.48×10^{-18}
$\text{CH}_2\text{OH}(X^2A'')$			
$\nu_1 (e)$	(CH_2, OH) twisting	426	9.73×10^{-18}
$\nu_2 (e)$	CH_2 wagging	566	1.71×10^{-17}
$\nu_3 (e)$	(CH_2, OH) twisting + scissoring	1030	7.87×10^{-18}
$\nu_4 (e)$	CO stretching	1170	1.56×10^{-17}
$\nu_5 (e)$	(CH_2, OH) rocking	1326	5.17×10^{-18}
$\nu_6 (e)$	CH_2 scissoring	1443	1.24×10^{-18}
$\nu_7 (e)$	CH_2 symmetric stretching	3018	3.77×10^{-18}
$\nu_8 (e)$	CH_2 asymmetric stretching	3159	3.18×10^{-18}
$\nu_9 (e)$	OH stretching	3724	8.18×10^{-18}
$\text{CH}_3\text{O}(X^2A')$			
$\nu_1 (a'')$	CO stretching	694	1.32×10^{-17}
$\nu_2 (a')$	CH_2 twisting + CH rocking	935	2.02×10^{-19}
$\nu_3 (a')$	CH_3 wagging	1076	1.52×10^{-18}
$\nu_4 (a'')$	CH_2 scissoring	1319	2.75×10^{-18}
$\nu_5 (a')$	CH_3 asymmetric stretching	1329	3.51×10^{-18}
$\nu_6 (a')$	CH_2 symmetric stretching + CH stretching	1473	7.94×10^{-19}
$\nu_7 (a')$	CH_2 asymmetric stretching	2803	2.84×10^{-20}
$\nu_8 (a')$	CO stretching	2866	7.42×10^{-18}
$\nu_9 (a'')$	CH_2 twisting + CH rocking	2905	7.73×10^{-18}
$\text{CH}_3(X^2A_2'')$			
$\nu_1 (a_2'')$	CH_3 wagging	492	1.40×10^{-17}
$\nu_2 (e')$	CH_2 scissoring	1361	6.86×10^{-19}
$\nu_3 (a_1')$	CH_2 symmetric stretching	3009	0
$\nu_4 (e')$	CH_2 asymmetric stretching	3183	1.15×10^{-18}
$\text{OH}(X^2\Pi)$			
$\nu_1 (\Sigma^+)$	OH stretching	3594	9.42×10^{-19}
$\text{H}_2\text{CO}(X^1A_1)$			
$\nu_1 (b_1)$	CH_2 wagging	1166	4.28×10^{-19}
$\nu_2 (b_2)$	CH_2 rocking	1232	2.44×10^{-18}
$\nu_3 (a_1)$	CH_2 scissoring	1493	1.32×10^{-18}
$\nu_4 (a_1)$	CO stretching + CH_2 scissoring	1772	1.83×10^{-17}
$\nu_5 (a_1)$	CH_2 symmetric stretching	2783	1.07×10^{-17}
$\nu_6 (b_2)$	CH_2 asymmetric stretching	2831	2.82×10^{-17}
$\text{trans-HCOH}(^1A')$			
$\nu_1 (a'')$	(OH + CH) rocking	1074	2.04×10^{-17}
$\nu_2 (a')$	(OH + CH) rocking	1185	2.27×10^{-17}
$\nu_3 (a')$	CO stretching	1289	9.98×10^{-18}
$\nu_4 (a')$	(OH + CH) rocking	1473	3.65×10^{-18}
$\nu_5 (a')$	CH stretching	2751	2.66×10^{-17}
$\nu_6 (a')$	OH stretching	3608	1.15×10^{-17}

TABLE A6—Continued

Bands	Characterization	Band Position (cm ⁻¹)	<i>A</i> (cm molecule ⁻¹)
cis-HCOH(¹ A')			
ν_1 (<i>a''</i>).....	(OH + CH) rocking	991	5.54×10^{-18}
ν_2 (<i>a'</i>).....	(OH + CH) rocking	1173	3.79×10^{-18}
ν_3 (<i>a'</i>).....	CO stretching	1295	1.01×10^{-17}
ν_4 (<i>a'</i>).....	(OH + CH) rocking	1433	9.03×10^{-18}
ν_5 (<i>a'</i>).....	CH stretching	2642	4.02×10^{-17}
ν_6 (<i>a'</i>).....	OH stretching	3417	4.62×10^{-18}
HCOH(³ A'')			
ν_1 (<i>e</i>).....	(OH + CH) rocking	443	1.43×10^{-17}
ν_2 (<i>e</i>).....	(OH + CH) rocking	1044	1.55×10^{-17}
ν_3 (<i>e</i>).....	(OH + CH) rocking	1122	1.06×10^{-17}
ν_4 (<i>e</i>).....	CO stretching	1261	4.04×10^{-18}
ν_5 (<i>e</i>).....	CH stretching	2955	3.63×10^{-18}
ν_6 (<i>e</i>).....	OH stretching	3563	5.79×10^{-18}
HCO(<i>X</i> ² A')			
ν_1 (<i>a'</i>).....	CH rocking	1078	6.66×10^{-18}
ν_2 (<i>a'</i>).....	CO stretching	1883	1.47×10^{-17}
ν_3 (<i>a'</i>).....	CH stretching	2543	1.57×10^{-17}
HOC(<i>X</i> ² A')			
ν_1 (<i>a'</i>).....	OH rocking	1096	1.37×10^{-17}
ν_2 (<i>a'</i>).....	CO stretching	1347	6.16×10^{-18}
ν_3 (<i>a'</i>).....	OH stretching	3173	1.04×10^{-17}
CH ₂ (<i>a</i> ¹ A ₁)			
ν_1 (<i>a</i> ₁).....	CH ₂ symmetric stretch	2797	1.53×10^{-17}
ν_2 (<i>a</i> ₁).....	bend	1363	0
ν_3 (<i>b</i> ₂).....	CH ₂ asymmetric stretch	2857	1.81×10^{-17}
CH ₂ (<i>X</i> ³ B ₁)			
ν_1 (<i>a</i> ₁).....	HCH bending	1025	2.03×10^{-18}
ν_2 (<i>a</i> ₁).....	(CH + CH) symmetric stretching	3023	1.24×10^{-19}
ν_3 (<i>b</i> ₂).....	(CH + CH) asymmetric stretching	3257	3.09×10^{-21}
H ₂ O(<i>X</i> ¹ A ₁)			
ν_1 (<i>a</i> ₁).....	HOH bending	1589	9.65×10^{-18}
ν_2 (<i>a</i> ₁).....	(OH + OH) symmetric stretching	3698	5.97×10^{-19}
ν_3 (<i>b</i> ₂).....	(OH + OH) asymmetric stretching	3793	4.16×10^{-18}
CH ₄ (<i>X</i> ¹ A ₁)			
ν_1 (<i>a</i> ₁).....	CH symmetric stretch	2937	0
ν_2 (<i>e</i>).....	CH bending	1514	0
ν_3 (<i>t</i>).....	CH asymmetric stretch	3041	4.64×10^{-18}
ν_4 (<i>t</i>).....	CH bending	1301	2.82×10^{-18}
CO(<i>X</i> ¹ Σ ⁺)			
ν_1 (Σ ⁺).....	CO stretching	2154	1.27×10^{-17}

NOTE.—The vibrational frequencies have been scaled by 0.97, to account for the anharmonicities; this factor is consistent with the B3LYP/6-311G(d,p) level of theory.

TABLE A7
CALCULATED VIBRATIONAL FREQUENCIES AND INTEGRAL ABSORPTION COEFFICIENTS OF VARIOUS SPECIES EXPECTED TO BE FORMED
VIA RADICAL-RADICAL RECOMBINATION REACTIONS AS LISTED IN TABLE 4

Bands	Characterization	Band Position (cm ⁻¹)	A (cm molecule ⁻¹)
CH₃OCH₃(X¹A_g)			
ν_1 (a_u)	COOC wagging	17	1.86×10^{-18}
ν_2 (a_u)	(CH ₃ + CH ₃) rocking	207	5.37×10^{-19}
ν_3 (a_g)	(CH ₃ + CH ₃) rocking simultaneously	258	0
ν_4 (a_u)	(CO + CO) rocking	293	1.90×10^{-18}
ν_5 (a_g)	(COO + OOC) scissoring	470	0
ν_6 (a_g)	OO stretching + (CH, CH) rocking	811	0
ν_7 (a_u)	(CO, CO) asymmetric stretching	1022	1.84×10^{-17}
ν_8 (a_g)	(CO, CO) symmetric stretching	1032	0
ν_9 (a_u)	(CH ₂ , CH ₂) twisting	1137	3.00×10^{-19}
ν_{10} (a_u)	(CH + CH) rocking + (CH ₂ + CH ₂) wagging	1138	1.85×10^{-18}
ν_{11} (a_g)	(CH ₂ + CH ₂) twisting	1142	0
ν_{12} (a_g)	(CH + CH) rocking + (CH ₂ + CH ₂) wagging + (CO + CO) stretching	1229	0
ν_{13} (a_u)	(CH ₃ + CH ₃) wagging	1402	7.28×10^{-19}
ν_{14} (a_g)	(CH ₃ + CH ₃) wagging simultaneously	1411	0
ν_{15} (a_g)	(CH ₂ + CH ₂) twisting simultaneously + (CH + CH) rocking	1411	0
ν_{16} (a_u)	(CH ₂ + CH ₂) twisting + (CH + CH) rocking	1412	2.31×10^{-18}
ν_{17} (a_u)	(CH ₂ + CH ₂) scissoring	1468	4.42×10^{-18}
ν_{18} (a_g)	(CH ₂ + CH ₂) scissoring simultaneously	1475	0
ν_{19} (a_u)	(CH ₃ + CH ₃) symmetric stretching	2910	1.72×10^{-17}
ν_{20} (a_g)	(CH ₃ + CH ₃) symmetric stretching simultaneously	2913	0
ν_{21} (a_g)	(CH ₂ + CH ₂) asymmetric stretching simultaneously	2970	0
ν_{22} (a_u)	(CH ₂ + CH ₂) asymmetric stretching	2970	1.75×10^{-17}
ν_{23} (a_u)	(CH, CH) asymmetric stretching	3019	5.70×10^{-18}
ν_{24} (a_g)	(CH, CH) symmetric stretching	3019	0
CH₃OCH₂OH(X¹A)			
ν_1 (e)	(CH ₂ , CH ₂) twisting	95	3.83×10^{-19}
ν_2 (e)	CH ₃ rocking	203	6.39×10^{-19}
ν_3 (e)	COC scissoring + CH of CH ₃ rocking + OH rocking	287	5.81×10^{-18}
ν_4 (e)	OH rocking + COC scissoring	367	1.67×10^{-17}
ν_5 (e)	OCO scissoring + OH rocking	513	2.71×10^{-18}
ν_6 (e)	COC symmetric stretching + CH of CH ₃ rocking + OH rocking	936	1.22×10^{-17}
ν_7 (e)	CH ₂ rocking + (CH of CH ₂ , OH) scissoring	1051	1.40×10^{-17}
ν_8 (e)	COC asymmetric stretching + CH of CH ₃ rocking	1085	1.21×10^{-17}
ν_9 (e)	CO of CH ₂ OH stretching + CO of OCH ₃ stretching	1101	3.61×10^{-17}
ν_{10} (e)	CH ₂ of CH ₃ twisting	1140	4.82×10^{-19}
ν_{11} (e)	CH ₂ of CH ₃ wagging + CH of CH ₃ rocking	1188	4.10×10^{-18}
ν_{12} (e)	CH ₂ twisting + OH rocking	1216	1.98×10^{-18}
ν_{13} (e)	(OH, CH of CH ₂) rocking	1355	2.84×10^{-18}
ν_{14} (e)	(CH ₂ + CH ₃) wagging	1405	1.02×10^{-17}
ν_{15} (e)	CH ₂ of CH ₃ scissoring + CH ₂ wagging	1437	2.12×10^{-18}
ν_{16} (e)	CH ₂ of CH ₃ scissoring + CH ₂ wagging	1445	2.28×10^{-18}
ν_{17} (e)	CH ₂ of CH ₃ scissoring + CH ₂ wagging	1465	1.01×10^{-18}
ν_{18} (e)	(CH ₂ + CH ₂ of CH ₃) scissoring	1496	1.99×10^{-19}
ν_{19} (e)	CH of CH ₂ stretching	2816	1.63×10^{-17}
ν_{20} (e)	CH ₂ of CH ₃ symmetric stretching + CH of CH ₃ stretching	2877	1.17×10^{-17}
ν_{21} (e)	CH ₂ of CH ₃ asymmetric stretching	2918	1.34×10^{-17}
ν_{22} (e)	CH of CH ₂ stretching	2922	1.12×10^{-17}
ν_{23} (e)	CH of CH ₃ stretching + CH ₂ of CH ₃ symmetric stretching	3026	4.41×10^{-18}
ν_{24} (e)	OH stretching	3699	4.86×10^{-18}
CH₃OCHO(X¹A')			
ν_1 (a'')	CH ₃ rocking	103	2.23×10^{-20}
ν_2 (a')	(OCH ₃ , CO of CHO) scissoring	291	2.34×10^{-18}
ν_3 (a'')	COC wagging + CH rocking	337	4.54×10^{-18}
ν_4 (a')	OCO scissoring + CH ₂ wagging + CH rocking	757	1.32×10^{-18}
ν_5 (a')	OC of OCH ₃ stretching	902	4.00×10^{-18}
ν_6 (a'')	CH of CHO rocking	1010	1.36×10^{-20}
ν_7 (a'')	CH ₂ of CH ₃ twisting + CH of CH ₃ rocking	1138	1.68×10^{-19}
ν_8 (a')	COC asymmetric stretching + CH ₂ of CH ₃ wagging + CH of CH ₃ rocking	1143	2.22×10^{-17}
ν_9 (a')	OC of OCHO stretching + OCH of OCH ₃ scissoring + CH ₂ wagging	1190	3.05×10^{-17}

TABLE A7—Continued

Bands	Characterization	Band Position (cm^{-1})	A (cm molecule^{-1})
ν_{10} (a')	CH of CHO rocking	1356	2.12×10^{-19}
ν_{11} (a')	CH_3 wagging	1425	7.82×10^{-19}
ν_{12} (a'')	CH_2 twisting + CH_2 scissoring	1440	1.68×10^{-18}
ν_{13} (a')	CH_2 scissoring + CH of CH_3 rocking	1454	1.77×10^{-18}
ν_{14} (a')	CO of CHO stretching	1757	4.81×10^{-17}
ν_{15} (a')	CH of CHO stretching	2940	1.19×10^{-17}
ν_{16} (a')	CH_3 symmetric stretching	2960	2.57×10^{-18}
ν_{17} (a'')	CH_2 asymmetric stretching	3029	3.73×10^{-18}
ν_{18} (a')	CH_2 symmetric stretching + CH of CH_3 stretching	3066	2.23×10^{-20}
$\text{HOCH}_2\text{CH}_2\text{OH}(X^1A)$			
ν_1 (e)	($\text{CH}_2 + \text{HOCH}_2$) rocking	132	2.44×10^{-18}
ν_2 (e)	OH rocking	233	1.85×10^{-17}
ν_3 (e)	OH rocking + HOCH_2 rocking	268	3.22×10^{-18}
ν_4 (e)	OH rocking	309	2.08×10^{-17}
ν_5 (e)	(OCC + CCO) scissoring	462	8.91×10^{-19}
ν_6 (e)	($\text{CH}_2 + \text{CH}_2$) rocking	805	3.59×10^{-19}
ν_7 (e)	HOC rocking	973	1.27×10^{-17}
ν_8 (e)	OCC symmetric stretching	1037	1.64×10^{-17}
ν_9 (e)	OC stretching	1039	9.31×10^{-18}
ν_{10} (e)	CH_2 rocking + CH_2 twisting + OH rocking	1066	6.55×10^{-20}
ν_{11} (e)	($\text{CH}_2 + \text{CH}_2$) rocking + OH rocking	1172	1.19×10^{-18}
ν_{12} (e)	HOCH_2 scissoring	1207	7.48×10^{-18}
ν_{13} (e)	($\text{CH}_2 + \text{CH}_2$) twisting	1272	1.24×10^{-18}
ν_{14} (e)	(CH + OH) rocking + OH scissoring	1331	2.07×10^{-18}
ν_{15} (e)	(CH + OH) scissoring	1362	4.69×10^{-18}
ν_{16} (e)	($\text{CH}_2 + \text{CH}_2$) wagging + OH scissoring	1423	2.31×10^{-19}
ν_{17} (e)	($\text{CH}_2 + \text{CH}_2$) scissoring simultaneously	1469	3.19×10^{-20}
ν_{18} (e)	($\text{CH}_2 + \text{CH}_2$) scissoring	1483	3.94×10^{-19}
ν_{19} (e)	CH stretching	2863	1.30×10^{-17}
ν_{20} (e)	(CH + CH) stretching simultaneously	2909	1.43×10^{-18}
ν_{21} (e)	(CH + CH) stretching + (CH + CH) stretching simultaneously	2925	1.64×10^{-17}
ν_{22} (e)	CH stretching	3005	6.32×10^{-18}
ν_{23} (e)	OH stretching	3714	3.35×10^{-18}
ν_{24} (e)	OH stretching	3734	4.91×10^{-18}
$\text{CH}_2\text{OHCHO}(X^1A')$			
ν_1 (a'')	(CH + CH_2 + OH) rocking	184	1.54×10^{-18}
ν_2 (a')	(CO, COH) scissoring + CH rocking	285	3.99×10^{-18}
ν_3 (a'')	OH rocking	379	1.46×10^{-17}
ν_4 (a'')	CH rocking + CH_2 twisting	703	1.56×10^{-20}
ν_5 (a')	OCC scissoring + (CC, COH) scissoring	744	1.66×10^{-18}
ν_6 (a')	CC stretching	836	8.58×10^{-18}
ν_7 (a'')	(CH + CH_2) rocking	1075	2.26×10^{-20}
ν_8 (a')	CO of COH stretching + OH rocking	1096	1.30×10^{-17}
ν_9 (a'')	CH_2 twisting + CH rocking	1207	4.38×10^{-19}
ν_{10} (a')	CH_2 wagging + OH rocking	1260	7.21×10^{-18}
ν_{11} (a')	CH_2 scissoring + OH rocking	1349	4.17×10^{-18}
ν_{12} (a')	CH_2 wagging + (OH + CH) rocking	1399	1.03×10^{-17}
ν_{13} (a')	CH_2 scissoring + OH rocking	1434	3.09×10^{-18}
ν_{14} (a')	CO of CHO stretching	1747	2.48×10^{-17}
ν_{15} (a')	CH of CHO stretching + CH_2 symmetric stretching	2831	1.30×10^{-17}
ν_{16} (a')	CH stretching + CH_2 symmetric stretching	2879	9.95×10^{-18}
ν_{17} (a'')	CH_2 asymmetric stretching	2890	4.83×10^{-18}
ν_{18} (a')	OH stretching	3601	9.92×10^{-18}
$\text{trans-CHOCHO}(X^1A_g)$			
ν_1 (a_u)	(HCO + HCO) twisting simultaneously	139	4.93×10^{-18}
ν_2 (b_u)	(HCO + HCO) rocking	323	8.57×10^{-18}
ν_3 (a_g)	(OCC + CCO) scissoring + CC stretching	536	0
ν_4 (a_u)	(CH + CH) asymmetric rocking	795	1.26×10^{-19}
ν_5 (a_g)	CC stretching	1025	0
ν_6 (b_g)	(CH + CH) symmetric rocking	1044	0
ν_7 (b_u)	(CH + CH) asymmetric rocking	1288	1.13×10^{-18}

TABLE A7—Continued

Bands	Characterization	Band Position (cm^{-1})	A (cm molecule^{-1})
$\nu_8 (a_g)$	(CH + CH) symmetric rocking	1335	0
$\nu_9 (b_u)$	(CO + CO) asymmetric stretching	1753	3.21×10^{-17}
$\nu_{10} (a_g)$	(CO + CO) symmetric stretching	1755	0
$\nu_{11} (b_u)$	(CH + CH) stretching	2835	2.77×10^{-17}
$\nu_{12} (a_g)$	(CH + CH) simultaneously stretching	2840	0
cis-CHOCHO(X^1A_1)			
$\nu_1 (a_2)$	(HCC + CCH) twisting	128	0
$\nu_2 (a_1)$	(HCO + HCO) rocking simultaneously	272	1.20×10^{-18}
$\nu_3 (b_1)$	H(CC)H wagging	718	8.20×10^{-21}
$\nu_4 (a_1)$	CC stretching	788	2.46×10^{-18}
$\nu_5 (b_2)$	(OCC + CCO) scissoring	799	1.28×10^{-17}
$\nu_6 (a_2)$	(HCC + CCH) wagging	1052	0
$\nu_7 (b_2)$	H(CC)H rocking	1346	1.27×10^{-19}
$\nu_8 (a_1)$	H(CC)H scissoring	1350	6.28×10^{-20}
$\nu_9 (a_1)$	(CO + CO) stretching simultaneously	1746	2.35×10^{-17}
$\nu_{10} (b_2)$	(CO + CO) stretching	1786	7.16×10^{-18}
$\nu_{11} (b_2)$	(CH + CH) stretching	2774	1.25×10^{-17}
$\nu_{12} (a_1)$	(CH + CH) stretching simultaneously	2809	3.04×10^{-17}
trans-HOCH = CHO(X^1A_g)			
$\nu_1 (a_u)$	(OH + OH) rocking	244	1.92×10^{-17}
$\nu_2 (b_g)$	(OH + OH) rocking	296	0
$\nu_3 (b_u)$	(HCO + HCO) rocking	309	6.07×10^{-18}
$\nu_4 (a_u)$	(HOC + HOC) wagging	365	1.54×10^{-17}
$\nu_5 (a_g)$	(OCC + OCC) scissoring	551	0
$\nu_6 (b_g)$	(HCC + HCC) wagging	776	0
$\nu_7 (a_u)$	(CH + CH) rocking	880	1.69×10^{-17}
$\nu_8 (a_g)$	(OH + OH) rocking	1049	0
$\nu_9 (b_u)$	(CO + CO) stretching	1109	7.29×10^{-17}
$\nu_{10} (b_u)$	(OH + OH + CH + CH) rocking	1181	5.45×10^{-19}
$\nu_{11} (a_g)$	(CH + CH) rocking	1292	0
$\nu_{12} (a_g)$	(OH + OH) rocking	1306	0
$\nu_{13} (b_u)$	(OH + OH + CH + CH) rocking	1372	1.52×10^{-17}
$\nu_{14} (a_g)$	CC stretching	1688	0
$\nu_{15} (a_g)$	(CH + CH) stretching simultaneously	3079	0
$\nu_{16} (b_u)$	(CH + CH) stretching	3080	5.88×10^{-18}
$\nu_{17} (b_u)$	(OH + OH) stretching	3702	9.84×10^{-18}
$\nu_{18} (a_g)$	(OH + OH) stretching simultaneously	3706	0
cis-HOCH = CHO(X^1A_1)			
$\nu_1 (b_1)$	(OH + OH) rocking	64	3.62×10^{-17}
$\nu_2 (a_2)$	(OH + OH) rocking	88	0
$\nu_3 (a_1)$	HO(CC)OH scissoring	235	7.17×10^{-19}
$\nu_4 (a_2)$	(OCC + CCO) wagging	517	0
$\nu_5 (b_1)$	(CH + CH) rocking	690	1.47×10^{-17}
$\nu_6 (b_2)$	(OCC + CCO) scissoring	708	6.09×10^{-18}
$\nu_7 (a_2)$	(CH + CH) rocking	805	0
$\nu_8 (a_1)$	(CO + CO) stretching	991	2.02×10^{-18}
$\nu_9 (b_2)$	(CO + CO) stretching	1085	2.80×10^{-17}
$\nu_{10} (a_1)$	(OH + OH) rocking	1186	2.71×10^{-17}
$\nu_{11} (b_2)$	(OH + OH) rocking	1270	1.78×10^{-17}
$\nu_{12} (a_1)$	(CH + CH) rocking	1276	1.23×10^{-17}
$\nu_{13} (b_2)$	(CH + CH) rocking	1403	4.45×10^{-18}
$\nu_{14} (a_1)$	CC stretching	1738	3.99×10^{-18}
$\nu_{15} (b_2)$	(CH + CH) stretching	3069	4.41×10^{-20}
$\nu_{16} (a_1)$	(CH + CH) stretching simultaneously	3093	4.72×10^{-18}
$\nu_{17} (b_2)$	(OH + OH) stretching	3759	2.64×10^{-17}
$\nu_{18} (a_1)$	(OH + OH) stretching simultaneously	3762	4.55×10^{-20}

TABLE A7—Continued

Bands	Characterization	Band Position (cm ⁻¹)	<i>A</i> (cm molecule ⁻¹)
CH₃COCH₃(<i>X</i>¹<i>A</i>)			
ν_1 (a).....	(CH ₃ + CH ₃) rocking	52	1.98×10^{-21}
ν_2 (b).....	(CH ₃ + CH ₃) rocking simultaneously	135	6.62×10^{-21}
ν_3 (a).....	CCC scissoring	366	1.91×10^{-19}
ν_4 (b).....	CCOC wagging + (CH ₂ + CH ₂) twisting	474	5.16×10^{-20}
ν_5 (b).....	(CH, CO) scissoring + (CO, CH) scissoring	519	2.49×10^{-18}
ν_6 (a).....	CCC symmetric stretching	756	2.50×10^{-19}
ν_7 (a).....	(CH ₂ + CH ₂) twisting	856	6.92×10^{-21}
ν_8 (b).....	(CH ₂ + CH ₂) wagging + CCC asymmetric stretching	857	1.57×10^{-18}
ν_9 (a).....	(CH ₂ + CH ₂) wagging + (CH, CH) scissoring	1051	5.91×10^{-21}
ν_{10} (b).....	CCOC wagging + (CH ₂ + CH ₂) rocking	1084	5.15×10^{-19}
ν_{11} (b).....	CCC asymmetric stretching + (CH, CH) rocking	1193	1.27×10^{-17}
ν_{12} (a).....	(CH ₃ + CH ₃) wagging simultaneously	1342	3.20×10^{-18}
ν_{13} (b).....	(CH ₃ + CH ₃) wagging	1344	1.07×10^{-17}
ν_{14} (b).....	(CH ₂ + CH ₂) scissoring + (CH, CH) rocking	1420	1.80×10^{-19}
ν_{15} (a).....	(CH ₂ + CH ₂) scissoring	1422	7.61×10^{-19}
ν_{16} (a).....	(CH ₂ + CH ₂) scissoring simultaneously + (CH, CH) scissoring	1427	3.96×10^{-18}
ν_{17} (b).....	(CH ₂ + CH ₂) twisting + (CH + CH) rocking	1443	3.69×10^{-18}
ν_{18} (a).....	CO stretching	1750	2.90×10^{-17}
ν_{19} (b).....	(CH ₃ + CH ₃) symmetric stretching	2934	3.38×10^{-19}
ν_{20} (a).....	(CH ₃ + CH ₃) symmetric stretching simultaneously	2940	1.14×10^{-18}
ν_{21} (a).....	(CH ₂ + CH ₂) asymmetric stretching	2988	7.48×10^{-20}
ν_{22} (b).....	(CH ₂ + CH ₂) asymmetric stretching simultaneously	2995	4.11×10^{-18}
ν_{23} (b).....	(CH, CH) asymmetric stretching	3046	2.15×10^{-18}
ν_{24} (a).....	(CH, CH) symmetric stretching	3047	1.65×10^{-18}
CH₃CH₂OH(<i>X</i>¹<i>A</i>)			
ν_1 (e).....	CH ₃ rocking	264	4.18×10^{-19}
ν_2 (e).....	OH rocking	309	1.89×10^{-17}
ν_3 (e).....	OCC scissoring	409	3.28×10^{-18}
ν_4 (e).....	(CH ₂ of CH ₃ + CH ₂) twisting	787	4.46×10^{-19}
ν_5 (e).....	CH of CH ₃ rocking + OCC symmetric stretching	859	1.73×10^{-18}
ν_6 (e).....	OCC asymmetric stretching	1029	1.84×10^{-18}
ν_7 (e).....	(CH of CH ₂ + CH of CH ₃ + OH) rocking + CH ₂ of CH ₃ wagging + CO stretching	1045	1.90×10^{-17}
ν_8 (e).....	(CH of CH ₂ + OH) rocking + CH ₂ of CH ₃ twisting	1103	7.06×10^{-19}
ν_9 (e).....	(CH ₂ of CH ₃ + CH ₂) twisting + OH rocking	1246	1.99×10^{-18}
ν_{10} (e).....	(CH of CH ₂ , OH) rocking + CH ₃ wagging	1339	2.56×10^{-19}
ν_{11} (e).....	CH ₃ wagging + (CH of CH ₂ + OH) rocking	1363	1.02×10^{-18}
ν_{12} (e).....	(CH ₃ + CH ₂) wagging + OH rocking	1383	7.52×10^{-18}
ν_{13} (e).....	CH ₂ of CH ₃ scissoring + CH ₂ of CH ₃ twisting	1443	1.41×10^{-18}
ν_{14} (e).....	(CH ₂ of CH ₃ + CH ₂) scissoring	1449	3.48×10^{-19}
ν_{15} (e).....	(CH ₂ + CH ₂ of CH ₃) scissoring	1475	9.54×10^{-20}
ν_{16} (e).....	CH of CH ₂ stretching	2889	1.23×10^{-17}
ν_{17} (e).....	CH ₃ symmetric stretching	2927	2.99×10^{-18}
ν_{18} (e).....	CH ₂ of CH ₃ symmetric stretching + (CH of CH ₃ , CH of CH ₂) symmetric stretching	2974	8.49×10^{-19}
ν_{19} (e).....	CH ₂ of CH ₃ asymmetric stretching + CH of CH ₂ stretching	2994	1.04×10^{-17}
ν_{20} (e).....	CH of CH ₃ stretching + CH ₂ of CH ₃ symmetric stretching + CH ₂ asymmetric stretching	3008	6.70×10^{-18}
ν_{21} (e).....	OH stretching	3710	2.80×10^{-18}

NOTE.—The vibrational frequencies have been scaled by 0.97, to account for the anharmonicities; this factor is consistent with the B3LYP/6-311G(d,p) level of theory.

REFERENCES

- Allamandola, L. J., Sandford, S. A., & Valero, G. J. 1988, *Icarus*, 76, 225
 Andersson, M. P., Uvdal, P., & MacKerell, A. D., Jr. 2002, *J. Phys. Chem. B*, 106, 5200
 Aspiala, A., Murto, J., & Sten, P. 1986, *Chem. Phys.*, 106, 399
 Baratta, G. A., Castorina, A. C., Leto, G., Palumbo, M. E., Spinella, F., & Strazzulla, G. 1994, *Planet. Space Sci.*, 42, 759
 Baratta, G. A., Leto, G., & Palumbo, M. E. 2002, *A&A*, 384, 343
 Becke, A. D. 1993, *J. Chem. Phys.*, 98, 5648
 Bennett, C. J., Jamieson, C. S., Osamura, Y., & Kaiser, R. I. 2005, *ApJ*, 624, 1097
 ———. 2006, *ApJ*, 653, 792
 Bertie, J. E., & Zhang, S. L. 1997, *J. Mol. Struct.*, 413–414, 333
 Blowers, P., Ford, L., & Masel, R. 1998, *J. Phys. Chem. A*, 102, 9267
 Brown, R. D., Crofts, J. G., Gardner, F. F., Godfrey, P. D., Robinson, B. J., & Whiteoak, J. B. 1975, *ApJ*, 197, L29
 Brunetto, R., Baratta, G. A., Domingo, M., & Strazzulla, G. 2005, *Icarus*, 175, 226
 Chang, A. H. H., & Lin, S. H. 2004, *Chem. Phys. Lett.*, 384, 229
 Charnley, S. B., Tielens, A. G. G. M., & Millar, T. J. 1992, *ApJ*, 399, L71
 Cheng, B.-M., Lee, Y.-P., & Ogilvie, J. F. 1988, *Chem. Phys. Lett.*, 151, 109
 Crovisier, J., Bockelée-Morvan, D., Biver, N., Colom, P., Despois, D., & Lis, D. C. 2004, *A&A*, 418, L35
 Cruikshank, D. P., Roush, T. L., & Poulet, F. 2003, *Comptes Rendus Physique*, 4, 783

- Cruikshank, D. P., et al. 1998, *Icarus*, 135, 389
- Dickens, J. E., & Irvine, W. M. 1997, *ApJ*, 489, 753
- DiSanti, M. A., Dello Russo, N., Magee-Sauer, K., Gibb, E. L., Reuter, D. C., & Mumma, M. J. 2002, in *Proc. Asteroids, Comets and Meteors*, ed. B. Warmbein (Noordwijk: ESA), 571
- Drouin, D., Couture, A. R., Gauvin, R., Hovington, P., Horny, P., & Demers, H. 2001, *Monte Carlo Simulation of Electron Trajectory in Solids (CASINO)* (ver. 2.42; Sherbrooke: Univ. Sherbrooke)
- Dunning, T. H. 1989, *J. Chem. Phys.*, 90, 1007
- Ehrenfreund, P., Charnley, S. B., & Wooden, D. 2004, in *Comets II*, ed. M. C. Festou, H. U. Keller, & H. A. Weaver (Tucson: Univ. Arizona Press), 115
- Falk, M., & Whalley, E. 1961, *J. Chem. Phys.*, 34, 1554
- Forney, D., Jacox, M. E., & Thompson, W. E. 2003, *J. Chem. Phys.*, 119, 20
- Fredin, L., Nelander, B., & Ribbegård, G. 1977, *J. Chem. Phys.*, 66, 4065
- Frenklach, M., Wang, H., & Rabinowitz, M. J. 1992, *Prog. Energy. Combustion Sci.*, 18, 47
- Frisch, M. J., et al. 2001, *Gaussian 98*, Rev. A.9 (Pittsburgh: Gaussian)
- Fuente, A., Neri, R., & Caselli, P. 2005, *A&A*, 444, 481
- Galabov, B., Yamaguchi, Y., Remington, R. B., & Schaefer, H. F., III. 2002, *J. Phys. Chem. A.*, 106, 819
- Garrod, R. T., & Herbst, E. 2006, *A&A*, 457, 927
- Gerakines, P. A., Schutte, W. A., & Ehrenfreund, P. 1996, *A&A*, 312, 289
- Gerakines, P. A., Schutte, W. A., Greenberg, J. M., & van Dishoeck, E. F. 1995, *A&A*, 296, 810
- Gibb, E. L., Whittet, D. C. B., Boogert, A. C. A., & Tielens, A. G. G. M. 2004, *ApJS*, 151, 35
- Gottlieb, C. A. 1973, in *Molecules in the Galactic Environment*, ed. M. A. Gordon & L. E. Snyder (New York: Wiley), 181
- Govender, M. G., & Ford, T. A. 2000, *J. Mol. Struct.*, 550–551, 445
- Grim, R. J. A., Baas, F., Geballe, T. R., Greenberg, J. M., & Schutte, W. 1991, *A&A*, 243, 473
- Harvey, K. B., & Ogilvie, J. F. 1962, *Canadian J. Chem.*, 40, 85
- Hiraoka, K., et al. 2005, *ApJ*, 620, 542
- Hollis, J. M., Lovas, F. J., & Jewell, P. R. 2000, *ApJ*, 540, L107
- Horn, A., Möllendal, H., Sekigucji, O., Uggerud, E., Roberts, H., Herbst, E., Viggiano, A. A., & Fridgen, T. D. 2004, *ApJ*, 611, 605
- Hudson, R. L., & Moore, M. H. 1999, *Icarus*, 140, 451
- . 2000, *Icarus*, 145, 661
- Hudson, R. L., Moore, M. H., & Cook, A. M. 2005, *Adv. Space Res.*, 36, 184
- Jacox, M. E. 1981, *Chem. Phys.*, 59, 213
- Jenniskens, P., Baratta, G. A., Kouchi, A., de Groot, M. S., Greenberg, J. M., & Strazzulla, G. 1993, *A&A*, 273, 583
- Johnson, R. E. 1990, *Energetic Charged Particle Interactions with Atmospheres and Surfaces* (Berlin: Springer)
- Jones, A. P. 2005, in *The Dusty and Molecular Universe*, ed. A. Wilson (Noordwijk: ESA), 239
- Kerkhof, O., Schutte, W. A., & Ehrenfreund, P. 1999, *A&A*, 346, 990
- Lee, C., Yang, W., & Parr, R. G. 1988, *Phys. Rev. B.*, 37, 785
- Lucas, S., Ferry, D., Demirdjian, B., & Suzanne, J. 2005, *J. Phys. Chem. B*, 109, 18103
- Maret, S., Ceccarelli, C., Tielens, A. G. G. M., Caux, E., Lefloch, B., Faure, A., Castets, A., & Flower, D. R. 2005, *A&A*, 442, 527
- Mehringer, D. M., Snyder, L. E., & Miao, Y. 1997, *ApJ*, 480, L71
- Mennella, V., Baratta, G. A., Esposito, A., Ferini, G., & Pendleton, Y. J. 2003, *ApJ*, 587, 727
- Milligan, D. E., & Jacox, M. E. 1967, *J. Chem. Phys.*, 47, 5146
- Moore, M. H., Ferrante, R. F., & Nuth, J. A., III 1996, *Planet. Space Sci.*, 44, 927
- Mumma, M. J., et al. 2005, *Science*, 310, 271
- Palumbo, M. E., Castorina, A. C., & Strazzulla, G. 1999, *A&A*, 342, 551
- Petraco, N. D. K., Allen, W. D., & Schaefer, H. F. 2002, *J. Chem. Phys.*, 116, 10229
- Prasad, S. S., & Tarafdar, S. P. 1983, *ApJ*, 267, 603
- Purvis, G. D., & Bartlett, R. J. 1982, *J. Chem. Phys.*, 76, 1910
- Raghavachari, K., Trucks, G. W., Pople, J. A., & Head-Gordon, M. 1989, *Chem. Phys. Lett.*, 157, 479
- Remijan, A. J., et al. 2006, *ApJ*, 643, 567
- Rodgers, S. D., & Charnley, S. B. 2001, *ApJ*, 546, 324
- . 2003, *ApJ*, 585, 355
- Sandford, S. A., & Allamandola, L. J. 1990, *ApJ*, 355, 357
- Sandford, S. A., Allamandola, L. J., Tielens, A. G. G. M., & Valero, G. J. 1988, *ApJ*, 329, 498
- Schöier, F. L., Jørgensen, J. K., van Dishoeck, E. F., & Blake, G. A. 2002, *A&A*, 390, 1001
- Serrallach, A., Meyer, R., & Günthard, Hs. H. 1974, *J. Mol. Spect.*, 52, 94
- Shiraki, T., Watanabe, N., Hidaka, H., & Kouchi, A. 2004, in *Proc. Joint AOGS 1st Annual Meetings and 2nd APHW Conference*, Vol. 1, ed. W.-H. Ip (Singapore: Asia Oceania Geosciences Soc.), 224
- Strazzulla, G., & Johnson, R. E. 1991, in *Comets in the Post-Halley Era*, ed. R. L. Newburn, Jr., M. Neugebauer, & J. Rahe (Dordrecht: Kluwer), 243
- Tauer, K. J., Lipscomb, Wm, N. 1952, *Acta Cryst*, 5, 606
- Turner, B. E., & Apponi, A. J. 2001, *ApJ*, 561, L207
- Wada, A., Mochizuki, N., & Hiraoka, K. 2006, *ApJ*, 644, 300
- Weber, A. L. 1998, *Origins of Life Evol. Biosphere*, 28, 259
- Wen, A. T., Michaud, M., & Sanche, L. 1998, *J. Electron Spectrosc. Related Phenom.*, 94, 23
- Woon, D. E. 2002, *ApJ*, 569, 541
- Yamada, H., & Person, W. B. 1964, *J. Chem. Phys.*, 41, 2478
- Yeom, Y. H., & Frie, H. 2003, *J. Chem. Phys. B*, 107, 6286
- Zhang, X., Zou, S., Harding, L. B., & Bowman, J. M. 2004, *J. Phys. Chem. A*, 108, 8980